Inorg. Chem. **2008**, *47*, 11032−11047

An Electrochemical Study of Antineoplastic Gallium, Iron and Ruthenium Complexes with Redox Noninnocent α-N-Heterocyclic Chalcogensemicarbazones

Christian R. Kowol,[†] Erwin Reisner,*[,†,‡] Ion Chiorescu,[†] Vladimir B. Arion,*[,†] Markus Galanski,[†] Dirk V. Deubel,[†] and Bernhard K. Keppler[†]

Institute of Inorganic Chemistry, University of Vienna, Währingerstrasse 42, A-1090 Vienna, Austria, and Inorganic Chemistry Laboratory, University of Oxford, South Parks Road, Oxford OX1 3QR, U.K.

Received July 16, 2008

The electrochemical properties of a series of α-N-heterocyclic chalcogensemicarbazones (HL), namely, thiosemicarbazones, selenosemicarbazones, and semicarbazones, and their gallium(III), iron(III), and ruthenium(III) complexes with the general formula $[ML_2][Y]$ (M = Ga, Fe or Ru; Y = PF_6^-, NO_3^-, or $FeCl_4^-$) were studied by cyclic voltammetry. The novel compounds were characterized by elemental analysis, a number of spectroscopic methods (NMR, UV−vis, IR), mass spectrometry and by X-ray crystallography. All complexes show several, mostly reversible, redox waves attributable to the reduction of the noninnocent chalcogensemicarbazone ligands at lower potentials (<−0.4 V vs NHE) than the metal-centered iron or ruthenium redox waves (>0 V vs NHE) in organic electrolyte solutions. The cyclic voltammograms of the gallium complexes display at least two consecutive reversible one-electron reduction waves. These reductions are shifted by ∼0.6 V to lower potentials in the corresponding iron and ruthenium complexes. The electrochemical, chemical, and spectroscopic data indicate that the ligand-centered reduction takes place at the $CH_3C{=}N$ double bond. Quantum chemical calculations on the geometric and electronic structures of 2-acetylpyridine $^4N,^4N$-dimethylthiosemicarbazone (HL^B), the corresponding metal complexes $[Ga(L^B)_2]^+$ and $[Fe^{II}(L^B)_2]$, and the one-electron reduction product for each of these species support the assignment of the reduction site and elucidate the observed order of the ligand-centered redox potentials, $E_{1/2}([Fe^{II}(L)_2]) < E_{1/2}(HL) < E_{1/2}([Ga(L)_2]^+)$. The influence of water on the redox potentials of the complexes is reported and the physiological relevance of the electrochemical data for cytotoxicity as well as for ribonucleotide reductase inhibitory capacity are discussed.

Introduction

Metal-based anticancer prodrugs may be activated selectively in the hypoxic tumor tissue upon reduction by biological reducing agents.[1,2] Electron-transfer can occur either to the metal-center, or, if in the biologically accessible range, to noninnocent ligands, resulting in reactive species capable of attacking biologically relevant target molecules either by ligand displacement at the low valent metal center or by radicals formed at the ligand entity, respectively. An *activation-by-reduction* step is thought to be important for platinum(IV) complexes that have been evaluated in clinical development, for example, tetraplatin ($[PtCl_4(1,2\text{-}(NH_2)_2\text{-}C_6H_{10})]$, abandoned), satraplatin ($[PtCl_2(OAc)_2(NH_3)(NH_2\text{-}C_6H_{11})]$, phase III), and iproplatin ($[PtCl_2(OH)_2(NH_2{}^iPr)_2]$, abandoned),[3] as well as for the activation of investigational ruthenium(III) prodrugs such as *trans*-$[RuCl_4(indazole)_2]^-$ (KP1019) and *trans*-$[RuCl_4(imidazole)(S\text{-DMSO})]^-$ (NAMI-A), both of which have already finished phase I clinical trials.[4−6] Indeed, an increasing metal-centered redox potential was shown to correlate with higher cytotoxicity for a series of platinum(IV)[7] and azole-based ruthenium(III) compounds.[8] Metal-centered redox potentials can be tuned and

* To whom correspondence should be addressed. Phone: +431427752615. Fax: +431427752680. E-mail: erwin.reisner@chem.ox.ac.uk (E.R.); vladimir.arion@univie.ac.at (V.B.A.).
† University of Vienna.
‡ University of Oxford.

(1) Reisner, E.; Arion, V. B.; Keppler, B. K.; Pombeiro, A. J. L. *Inorg. Chim. Acta* **2008**, *361*, 1569–1583.
(2) Clarke, M. J.; Zhu, F.; Frasca, D. R. *Chem. Rev.* **1999**, *99*, 2511–2533.
(3) Hall, M. D.; Hambley, T. W. *Coord. Chem. Rev.* **2002**, *232*, 49–67.

10.1021/ic8013249 CCC: $40.75
Published on Web 10/31/2008

predicted by application of Lever's parametrization method, facilitating markedly the design of bioreductive drugs.[1,9,10] Although hypoxia-selective organic drugs are under intensive investigation, for example, nitroimidazoles,[11] little is known about reductively activated metal-based compounds containing electronically noninnocent ligands with physiologically accessible redox potentials. One such example is ferrocenyl hydroxytamoxifen, containing a ferrocene-moiety attached to a hydroxylated form of the estrogen receptor modulator tamoxifen, which shows high activity on estrogen receptor positive and negative cell lines.[12,13]

Thiosemicarbazones are versatile redox noninnocent ligands with a wide range of coordination modes in metal complexes, in particular, when their binding capacity is further increased by condensation of the thiosemicarbazide with an aldehyde or ketone containing an additional donor atom in a suitable position for chelation.[14] In addition to their exciting coordination chemistry, thiosemicarbazones have evoked considerable interest because of their broad spectrum of pharmacological activity. In particular, α-N-heterocyclic thiosemicarbazones were found to possess antitumor, antimalarial, antibacterial, antifungal, and antiviral activity,[15] and ^{64}Cu-bis(thiosemicarbazonate) complexes are under investigation as hypoxia-selective positron emission tomography tracers.[16] The enzyme ribonucleotide reductase (RR) has been identified as the principal molecular target.[17] Ribonucleotide reductase converts ribonucleotides to deoxyribonucleotides necessary for DNA synthesis and is highly expressed in tumor cells making it a suitable and well established target in cancer chemotherapy.[18] Initially, the inhibition of RR was attributed to the ability of thiosemicarbazones as strong chelators to remove iron from the enzyme active site, but later, it was found that preformed iron chelates of some thiosemicarbazones with a terminal NH_2 group ($^4NH_2$) show higher RR inhibitory activity than the uncomplexed thiosemicarbazones.[19−21] This is in agreement with data on 3-aminopyridine-2-carboxaldeyde thiosemicarbazone (Triapine), an investigational drug currently in phase II clinical trials, where an increase in cytotoxicity upon coordination to iron was found.[22]

We reported previously that in the presence of the reductant dithiothreitol (DTT) iron(III) complexes with ^{4}N-disubstituted α-N-heterocyclic thiosemicarbazone ligands show the fastest destruction of the R2 specific tyrosine free radical in mouse RR followed by the metal-free ligands and the corresponding gallium(III) complexes.[23] In the absence of DTT, no tyrosyl radical quenching was observed. The cytotoxicity data for the same compounds tested in the cancer cell lines 41 M (ovarian carcinoma) and SK-BR-3 (mammary carcinoma) are in reversed order: the gallium complexes exhibited slightly higher cytotoxicity in the low nanomolar range in comparison to the metal-free ligand, whereas the iron(III) complexes displayed a much lower cytotoxicity in the micromolar range. Thus, iron is essential for the fast quenching of the tyrosyl radical in RR, but it is not solely responsible for the antitumor potency of the ^{4}N-disubstituted thiosemicarbazone derivatives suggesting the existence of additional molecular targets. The requirement of an adequate reductant (e.g., DTT) for successful radical quenching indicates that the iron(III) complex is reduced to its iron(II) form prior radical quenching.

These findings prompted us to prepare a series of gallium(III), iron(III), and ruthenium(III) complexes of the general formula $[ML_2][Y]$ (M = Ga, Fe and Ru; Y = PF_6^-, NO_3^- or $FeCl_4^-$), where HL is a chalcogensemicarbazone ligand (Charts 1 and 2), and to investigate the effect of coordination to the metal on their metal- and ligand-centered redox properties by carrying out detailed electrochemical investigations and quantum chemical calculations. We were particularly interested to clarify if the redox properties/potentials of the prepared compounds are of physiological relevance, that is, to elucidate whether a relation between their electrochemical properties and antiproliferative activity or R2 specific tyrosine free radical quenching ability can be found.

Experimental Section

All solvents and reagents were obtained from commercial suppliers and used without further purification. The ligands **HL^A**, **HL^B**, **HL^E**−**HL^G** and complexes **1A**, **1B**, **1E**−**1G**, **2A**, **2B**, **2E**−**2G**, **2′A**−**2′G**,[23] as well as **HL^J**, **HL^K**, **1J**, **1K**, **3B**,[24] and **HL^D**[25] were prepared as described previously. **HL^C** was synthesized

(4) Alessio, E.; Mestroni, G.; Bergamo, A.; Sava, G. *Curr. Top. Med. Chem.* **2004**, *4*, 1525–1535.
(5) Clarke, M. J. *Coord. Chem. Rev.* **2003**, *236*, 209–233.
(6) Hartinger, C. G.; Zorbas-Seifried, S.; Jakupec, M. A.; Kynast, B.; Zorbas, H.; Keppler, B. K. *J. Inorg. Biochem.* **2006**, *100*, 891–904.
(7) Hall, M. D.; Amjadi, S.; Zhang, M.; Beale, P. J.; Hambley, T. W. *J. Inorg. Biochem.* **2004**, *98*, 1614–1624.
(8) Jakupec, M. A.; Reisner, E.; Eichinger, A.; Pongratz, M.; Arion, V. B.; Galanski, M.; Hartinger, C. G.; Keppler, B. K. *J. Med. Chem.* **2005**, *48*, 2831–2837.
(9) Lever, A. B. P. *Inorg. Chem.* **1990**, *29*, 1271–1285.
(10) Reisner, E.; Arion, V. B.; Eichinger, A.; Kandler, N.; Giester, G.; Pombeiro, A. J. L.; Keppler, B. K. *Inorg. Chem.* **2005**, *44*, 6704–6716.
(11) Brown, J. M. *Cancer Res.* **1999**, *59*, 5863–5870.
(12) Top, S.; Tang, J.; Vessieres, A.; Carrez, D.; Provot, C.; Jaouen, G. *Chem. Commun.* **1996**, 955–956.
(13) Hillard, E.; Vessieres, A.; Thouin, L.; Jaouen, G.; Amatore, C. *Angew. Chem., Int. Ed.* **2006**, *45*, 285–290.
(14) (a) Gerbeleu, N. V.; Arion, V. B.; Burgess, J. *Template Synthesis of Macrocyclic Compunds*, Wiley-VCH: Weinheim, Germany, 1999; Chapter 2. (b) Casas, J. S.; Garcia-Tasende, M. S.; Sordo, J. *Coord. Chem. Rev.* **2000**, *209*, 197–261.
(15) West, D. X.; Padhye, S. B.; Sonawane, P. B. *Struct. Bonding (Berlin)* **1991**, *76*, 1–50.
(16) Bonnitcha, P. D.; Vavere, A. L.; Lewis, J. S.; Dilworth, J. R. *J. Med. Chem.* **2008**, *51*, 2985–2991.
(17) Moore, E. C.; Zedeck, M. S.; Agrawal, K. C.; Sartorelli, A. C. *Biochemistry* **1970**, *9*, 4492–4498.
(18) Shao, J.; Zhou, B.; Chu, B.; Yen, Y. *Curr. Cancer Drug Targets* **2006**, *6*, 409–431.
(19) Saryan, L. A.; Ankel, E.; Krishnamurti, C.; Petering, D. H. *J. Med. Chem.* **1979**, *22*, 1218–1221.
(20) Preidecker, P. J.; Agrawal, K. C.; Sartorelli, A. C.; Moore, E. C. *Mol. Pharmacol.* **1980**, *18*, 507–512.
(21) Thelander, L.; Gräslund, A. *J. Biol. Chem.* **1983**, *258*, 4063–4066.
(22) Finch, R. A.; Liu, M.-C.; Cory, A. H.; Cory, J. G.; Sartorelli, A. C. *Adv. Enzyme Regul.* **1999**, *39*, 3–12.
(23) Kowol, C. R.; Berger, R.; Eichinger, R.; Roller, A.; Jakupec, M. A.; Schmidt, P. P.; Arion, V. B.; Keppler, B. K. *J. Med. Chem.* **2007**, *50*, 1254–1265.
(24) Kowol, C. R.; Eichinger, R.; Jakupec, M. A.; Galanski, M.; Arion, V. B.; Keppler, B. K. *J. Inorg. Biochem.* **2007**, *101*, 1946–1957.
(25) West, D. X.; Ingram, J. J., III.; Kozub, N. M.; Bain, G. A.; Liberta, A. E. *Transition Met. Chem.* **1996**, *21*, 213–218.

Chart 1. Chalcogensemicarbazone Ligands Used in This Study

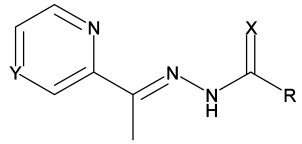

X = S, Y = CH, R = $N(C_4H_8)$ (**HL^A**)

X = S, Y = CH, R = $N(CH_3)_2$ (**HL^B**)

X = S, Y = CH, R = $NH(C_6H_5)$ (**HL^C**)

X = S, Y = CH, R = $NH(p\text{-}C_6H_4NO_2)$ (**HL^D**)

X = S, Y = N, R = $N(C_4H_8)$ (**HL^E**)

X = S, Y = N, R = $N(C_5H_{10})$ (**HL^F**)

X = S, Y = N, R = $N(CH_3)_2$ (**HL^G**)

X = S, Y = N, R = $NH(C_6H_5)$ (**HL^H**)

X = S, Y = N, R = $NH(p\text{-}C_6H_4NO_2)$ (**HL^I**)

X = O, Y = CH, R = $N(CH_3)_2$ (**HL^J**)

X = Se, Y = CH, R = $N(CH_3)_2$ (**HL^K**)

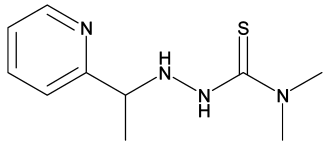

(**HL^M**)

Chart 2. Library of Metal Chalcogensemicarbazonate Complexes

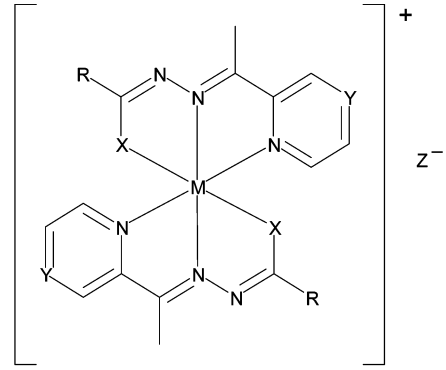

$[ML_2][Z]$

M = Ga, L = L^A, Z = PF_6 (**1A**) M = Fe, L = L^A, Z = PF_6 (**2A**)

M = Ga, L = L^B, Z = PF_6 (**1B**) M = Fe, L = L^B, Z = PF_6 (**2B**)

M = Ga, L = L^C, Z = PF_6 (**1C**) M = Fe, L = L^C, Z = PF_6 (**2C**)

M = Ga, L = L^D, Z = NO_3 (**1D**) M = Fe, L = L^D, Z = NO_3 (**2D**)

M = Ga, L = L^E, Z = PF_6 (**1E**) M = Fe, L = L^E, Z = PF_6 (**2E**)

M = Ga, L = L^F, Z = PF_6 (**1F**) M = Fe, L = L^F, Z = PF_6 (**2F**)

M = Ga, L = L^G, Z = PF_6 (**1G**) M = Fe, L = L^G, Z = PF_6 (**2G**)

M = Ga, L = L^H, Z = NO_3 (**1H**) M = Fe, L = L^H, Z = NO_3 (**2H**)

M = Ga, L = L^I, Z = NO_3 (**1I**) M = Fe, L = L^I, Z = NO_3 (**2I**)

M = Ga, L = L^J, Z = PF_6 (**1J**) M = Fe, L = L^A, Z = $FeCl_4$ (**2'A**)

M = Ga, L = L^K, Z = PF_6 (**1K**) M = Fe, L = L^B, Z = $FeCl_4$ (**2'B**)

M = Fe, L = L^E, Z = $FeCl_4$ (**2'E**)

M = Fe, L = L^F, Z = $FeCl_4$ (**2'F**)

M = Fe, L = L^G, Z = $FeCl_4$ (**2'G**)

M = Ru, L = L^B, Z = PF_6 (**3B**)

by condensation of equimolar amounts of ^4N-phenylthiosemicarbazide and 2-acetylpyridine in boiling ethanol in 60% yield. Acetylpyrazine hydrazone was obtained by reacting acetylpyrazine with an excess of hydrazine hydrate as the reagent and solvent at room temperature for 24 h.

Elemental analyses were carried out on a Carlo Erba microanalyzer at the Microanalytical Laboratory of the University of Vienna. Electrospray ionization mass spectrometry was carried out with a Bruker Esquire 3000 instrument (Bruker Daltonic, Bremen, Germany). Expected and experimental isotope distributions were compared. Infrared spectra were obtained from KBr pellets with a Perkin-Elmer FT-IR 2000 instrument (4000−400 cm^{-1}). UV−vis spectra were recorded on a Perkin-Elmer Lambda 650 spectrophotometer using samples dissolved in methanol (900−210 nm). The iron complexes were measured on a Hewlett-Packard 8453 UV−vis spectrophotometer (1100−210 nm). Thermogravimetric analysis (TGA) and differential thermal analysis (DTA) measurements were carried out simultaneously with a Mettler Toledo TGA/SDTA851e apparatus, with a 3 °C/min heating rate under an air atmosphere. ^1H, ^{13}C, and ^{15}N one- and two-dimensional NMR spectra were recorded by using DMSO-d_6 as the solvent with a Bruker DPX 400 or a 500 MHz Bruker FT-NMR spectrometer Avance III. The residual ^1H and ^{13}C present in DMSO-d_6 were used as internal references. ^{15}N NMR chemical shifts were referenced relative to ammonium chloride as the external standard. Abbreviations for NMR data: py = pyridine, pz = pyrazine, ph = phenyl or *p*-nitrophenyl, $C_{q,py}$ = quaternary carbon of pyridine, $C_{q,pz}$ = quaternary carbon of pyrazine, $C_{q,ph}$ = quaternary carbon of phenyl or *p*-nitrophenyl.

Electrochemistry. Cyclic voltammograms were measured in a three-electrode cell using a 2.0 mm-diameter glassy carbon or platinum disk working electrode, a platinum auxiliary electrode, and a $Ag|Ag^+$ reference electrode containing 0.10 M $AgNO_3$, the potential of which was corrected using an internal standard of ferrocenium/ferrocene. Measurements were performed at room temperature using an EG&G PARC 273A potentiostat/galvanostat. Deaeration of solutions was accomplished by passing a stream of argon through the solution for 5 min prior to the measurement and then maintaining a blanket atmosphere of argon over the solution during the measurement. Square wave voltammograms (SWVs) were recorded at 2 mV step height, 25 mV pulse, and a frequency of 100 Hz (scan rate 100 mV/s). The potentials were measured in 0.20 M $[n\text{-}Bu_4N][BF_4]/CH_3CN$, using $[Fe(\eta^5\text{-}C_5H_5)_2]$ ($E_{1/2}$ = +0.69 V vs. NHE)[26] as internal standard, and are quoted relative to the normal hydrogen electrode (NHE). **HL^C**, **HL^G**, and the nitro group containing compounds **HL^D**, **HL^I**, **1D**, **1I**, **2D**, and **2I** were

(26) Barette, W. C., Jr.; Johnson, H. W., Jr.; Sawyer, D. T. *Anal. Chem.* **1984**, *56*, 1890–1898.

measured in 0.20 M [*n*-Bu_4N][BF_4]/DMF ($E_{1/2}$ = +0.72 V vs NHE)[26] because of their low solubility in CH_3CN. For the cyclic voltammetry measurement in 0.15 M [*n*-Bu_4N][BF_4] in CH_3CN/H_2O or DMF/H_2O (7:3 v/v), a 2.0 mm-diameter glassy carbon working electrode, a platinum auxiliary electrode, and a Ag|Ag^+ reference electrode containing 3 M NaCl were used.

Synthesis of Ligands and Metal Complexes. Acetylpyrazine ^{4}*N*-Phenylthiosemicarbazone (HL^H). To ^{4}*N*-phenylthiosemicarbazide[27] (500 mg, 3.0 mmol) in boiling ethanol (15 mL) acetylpyrazine (365 mg, 3.0 mmol) was added, and the mixture was stirred under reflux for 5 h. After the reaction mixture was cooled to room temperature, the white solid was filtered off, washed with ethanol, and dried in vacuo. Yield: 590 mg (73%). Anal. Calcd for $C_{13}H_{13}N_5S$ (M_r = 271.34 g/mol): C, 57.54; H, 4.83; N, 25.81. Found: C, 57.45; H, 4.86; N, 25.56. ESI-MS in MeOH (positive): *m*/*z* 294, $[HL^H + Na]^+$. ESI-MS in MeOH (negative): *m*/*z* 270, $[HL^H - H]^-$. IR spectrum in KBr, cm^{-1} (selected bands): 3305 s, 3217 s, 1588 m, 1528 s, 1517 s, 1469 s, 1445 s, 1362 m, 1304 m, 1259 m, 1190 s, 1169 s, 1014 m, 854 s, 806 m, 749 s, 690 s, 590 m, 555 m. UV−vis (MeOH), λ_{max}, nm (ε, M^{-1} cm^{-1}): 251 (10020), 326 (27950), 420sh (1930). ^{1}H NMR (400.13 MHz, DMSO-d_6): δ 10.84 (s, 1H, N−NH) 10.33 (s, 1H, NH), 9.79 (d, $^4J_{H,H}$ = 1.0 Hz, 1H, pz), 8.65−8.63 (m, 2H, pz), 7.53 (d, $^3J_{H,H}$ = 7.6 Hz, 2H, ph), 7.40 (t,$^3J_{H,H}$ = 7.6 Hz, 2H, ph), 7.25 (t, $^3J_{H,H}$ = 7.6 Hz, 1H, ph), 2.45 (s, 3H, CH_3) ppm. ^{13}C NMR (125.81 MHz, DMSO-d_6): δ 178.0 (C═S), 150.4 ($C_{q,pz}$), 147.6 (*C*═N), 144.6 (C_{pz}), 144.0 (C_{pz}), 143.6 (C_{pz}), 139.6 ($C_{q,ph}$), 128.6 (C_{ph}), 127.0 (C_{ph}), 126.2 (C_{ph}), 12.7 (CH_3) ppm. Single crystals suitable for X-ray data collection were obtained from a methanolic solution of HL^H saturated with dichloromethane.

Acetylpyrazine ^{4}*N*-*p*-Nitrophenylthiosemicarbazone (HL^I). To acetylpyrazine hydrazone (300 mg, 2.20 mmol) in acetonitrile (7 mL) *p*-nitrophenyl isothiocyanate (397 mg, 2.20 mmol) in acetonitrile (6 mL) was added, and the reaction mixture was allowed to stir for 2 h at room temperature. The pale-yellow solid formed was filtered off, washed with acetonitrile, and dried in vacuo. Yield: 520 mg (75%). Anal. Calcd for $C_{13}H_{12}N_6O_2S$ (M_r = 316.34 g/mol): C, 49.36; H, 3.82; N, 26.57. Found: C, 49.51; H, 3.85; N, 26.44. ESI-MS in MeOH (negative): *m*/*z* 315, $[HL^I - H]^-$. IR spectrum in KBr, cm^{-1} (selected bands): 3274 m, 3209 m, 3063 m, 1598 m, 1558 s, 1492 s, 1466 m, 1330 s, 1289 m, 1013 m, 850 s, 806 s, 751 m, 698 m, 625 m. UV−vis (MeOH), λ_{max}, nm (ε, M^{-1} cm^{-1}): 333 (34500), 424sh (3430). ^{1}H NMR (500.32 MHz, DMSO-d_6): δ 11.25 (s, 1H, N−NH), 10.58 (s, 1H, NH), 9.75 (d, $^4J_{H,H}$ = 1.0 Hz, 1H, pz), 8.68−8.66 (m, 2H, pz), 8.27 (m, 2H, ph), 8.00 (m, 2H, ph), 2.48 (s, 3H, CH_3) ppm. ^{13}C NMR (125.81 MHz, DMSO-d_6): δ 177.4 (C═S), 150.2 ($C_{q,pz}$), 148.9 (*C*═N), 145.8 ($C_{q,ph}$), 144.8 (C_{pz}), 144.3 ($C_{q,\ ph}$), 144.0 (C_{pz}), 143.7 (C_{pz}), 125.8 (C_{ph}), 124.1 (C_{ph}), 13.0 (CH_3) ppm.

***N*,*N*-Dimethyl-2-(1-pyridin-2-ylethyl)hydrazinecarbothioamide (HL^M).** The ligand was prepared following the literature protocol.[28] Anal. Calcd for $C_{10}H_{16}N_4S$ (M_r = 224.33 g/mol): C, 53.54; H, 7.19; N, 24.98; S, 14.29. Found: C, 53.49; H, 7.35; N, 25.11; S, 14.19. ESI-MS in MeOH (negative): *m*/*z* 223, $[HL^M - H]^-$. IR spectrum in KBr, cm^{-1} (selected bands): 3225 m, 3167 m, 2960 m, 1597 m, 1514 s, 1437 m, 1378 s, 1320 s, 1146 m, 1115 m, 1002 m, 963 m, 915 m, 828 m, 789 s, 662 m, 547 m. UV−vis (MeOH), λ_{max}, nm (ε, M^{-1} cm^{-1}): 246 (15030). ^{1}H NMR (500.10 MHz, DMSO-d_6): δ 8.88 (d, $^3J_{NH,NH}$ = 5.7 Hz, 1H, S═CN*H*), 8.50 (m, 1H, py), 7.77 (dt, $^3J_{H,H}$ = 7.6 Hz, $^4J_{H,H}$ = 1.9 Hz, 1H, py), 7.53 (d, $^3J_{H,H}$ = 7.9 Hz, 1H, py), 7.26 (m, 1H, py), 5.69 (dd, $^3J_{NH,NH}$ = 5.7 Hz, $^3J_{NH,CH}$ = 3.2 Hz, 1H, CHN*H*), 4.11 (dq, $^3J_{H,H}$ = 6.6 Hz, $^3J_{NH,CH}$ = 3.2 Hz, 1H, CH), 3.08 (s, 6H, $N(CH_3)_2$), 1.30 (d, $^3J_{H,H}$ = 6.6 Hz, 3H, CCH_3) ppm. ^{13}C NMR (125.81 MHz, DMSO-d_6): δ 182.8 (C═S), 163.0 ($C_{q,py}$), 149.2 (C_{py}), 137.0 (C_{py}), 122.7 (C_{py}), 121.7 (C_{py}), 61.0 (CH), 40.6 ($N(CH_3)_2$), 20.0 (CCH_3) ppm. ^{15}N NMR (50.70 MHz, DMSO-d_6): δ 291.2 (N_{py}), 116.7 ($^1J_{N,H}$ = 98 Hz, CHNH), 76.8 ($^1J_{N,H}$ = 78 Hz, NH), 72.5 ($N(CH_3)_2$) ppm. Single crystals suitable for X-ray data collection were obtained by slow evaporation of a methanolic solution of HL^M.

[Bis(2-acetylpyridine ^{4}*N*-Phenylthiosemicarbazonato)-*N*,*N*,*S*-gallium(III)]hexafluorophosphate Monohydrate, $[Ga(L^C)_2]PF_6 \cdot H_2O$ (1C). To 2-acetylpyridine ^{4}*N*-phenylthiosemicarbazone (HL^C) (50 mg, 0.185 mmol) in dry ethanol (5 mL) at room temperature gallium(III) nitrate nonahydrate (40 mg, 0.096 mmol) in ethanol (2 mL) was added, and the reaction mixture was allowed to stir for 2 h. The solution was filtered to remove undissolved material, and ammonium hexafluorophosphate (60 mg, 0.37 mmol) was added to the filtrate. The yellow solid formed was filtered off after 30 min, washed with ethanol, and dried in vacuo. Yield: 50 mg (70%). Anal. Calcd for $C_{28}H_{26}F_6GaN_8PS_2 \cdot H_2O$ (M_r = 771.39 g/mol): C, 43.60; H, 3.66; N, 14.53. Found: C, 43.28; H, 3.53; N, 14.44. ESI-MS in MeOH (positive): *m*/*z* 607, $[Ga(L^C)_2]^+$; ESI-MS in MeOH (negative): *m*/*z* 145, $[PF_6]^-$. IR spectrum in KBr, cm^{-1} (selected bands): 3389 m, 1598 m, 1498 m, 1457 s, 1429 s, 848 vs, 558 m. UV−vis (MeOH), λ_{max}, nm (ε, M^{-1} cm^{-1}): 230sh (32670), 254 (31090), 263sh (29710), 300 (15850), 405 (43350). ^{1}H NMR (400.13 MHz, DMSO-d_6): δ 10.26 (s, 2H, NH), 8.36 (d, $^3J_{H,H}$ = 7.8 Hz, 2H, py), 8.30 (m, 2H, py), 8.10 (d, $^3J_{H,H}$ = 5.1 Hz, 2H, py), 7.79 (d, $^3J_{H,H}$ = 8.1 Hz, 4H, ph), 7.67 (m, 2H, py), 7.38 (t, $^3J_{H,H}$ = 8.1 Hz, 4H, ph), 7.10 (t, $^3J_{H,H}$ = 7.3 Hz, 2H, ph), 2.95 (s, 6H, CH_3) ppm. ^{13}C NMR (100.63 MHz, DMSO-d_6): δ 172.5 (C−S), 152.1 (*C*═N), 145.6 ($C_{q,py}$), 145.6 (C_{py}), 143.4 (C_{py}), 140.5 ($C_{q,ph}$), 129.6 (C_{ph}), 128.8 (C_{py}), 125.7 (C_{py}), 124.4 (C_{ph}), 122.2 (C_{ph}), 16.1 (CH_3) ppm.

[Bis(2-acetylpyridine ^{4}*N*-*p*-Nitrophenylthiosemicarbazonato)-*N*,*N*,*S*-gallium(III)]nitrate Monohydrate, $[Ga(L^D)_2]NO_3 \cdot H_2O$ (1D). To 2-acetylpyridine ^{4}*N*-*p*-nitrophenylthiosemicarbazone (HL^D) (100 mg, 0.32 mmol) in boiling methanol (25 mL) gallium(III) nitrate nonahydrate (67 mg, 0.16 mmol) in methanol (2 mL) was added, and the reaction mixture was stirred under reflux for 1 h. The yellow solid was separated from the hot solution by filtration, washed with methanol, and dried in vacuo. Yield: 50 mg (41%). Anal. Calcd for $C_{28}H_{24}GaN_{11}O_7S_2 \cdot H_2O$ (M_r = 778.43 g/mol): C, 43.20; H, 3.37; N, 19.79. Found: C, 43.04; H, 3.40; N, 19.56. ESI-MS in MeOH (positive): *m*/*z* 697, $[Ga(L^D)_2]^+$. ESI-MS in MeOH (negative): *m*/*z* 695, $[Ga(L^D)_2 - 2H]^-$. IR spectrum in KBr, cm^{-1} (selected bands): 3078 w, 1574 s, 1495 s, 1437 s, 1404 m, 1324 s, 1302 s, 1260 s, 1108 s, 848 m, 750 m. UV−vis (MeOH), λ_{max}, nm (ε, M^{-1} cm^{-1}): 251sh (24650), 296sh (19880), 330sh (26520), 396 (66330), 409sh (62220). ^{1}H NMR (400.13 MHz, DMSO-d_6): δ 10.77 (s, 2H, NH), 8.48 (d, $^3J_{H,H}$ = 8.1 Hz, 2H, py), 8.35 (m, 2H, py), 8.31 (m, 4H, ph), 8.18 (d, $^3J_{H,H}$ = 4.8 Hz, 2H, py), 8.08 (m, 4H, ph), 7.73 (m, 2H, py), 3.03 (s, 6H, CH_3) ppm. ^{13}C NMR (100.63 MHz, DMSO-d_6): δ 172.4 (C−S), 155.7 (*C*═N), 146.5 ($C_{q,ph}$), 145.9 (C_{py}), 145.3 ($C_{q,py}$), 143.7 (C_{py}), 142.6 ($C_{q,ph}$), 129.5 (C_{py}), 126.4 (C_{py}), 125.8 (C_{ph}), 121.3 (C_{ph}), 16.7 (CH_3) ppm.

[Bis(acetylpyrazine ^{4}*N*-Phenylthiosemicarbazonato)-*N*,*N*,*S*-gallium(III)]nitrate Monohydrate, $[Ga(L^H)_2]NO_3 \cdot H_2O$ (1H). To acetylpyrazine ^{4}*N*-phenylthiosemicarbazone (HL^H) (100 mg, 0.37 mmol) in boiling methanol (5 mL) gallium(III) nitrate nonahydrate (80 mg, 0.19 mmol) in methanol (3 mL) was added, and the mixture was stirred under reflux for 4 h. The yellow solid was

(27) Pulvermacher, G. *Chem. Ber.* **1893**, *26*, 613–630.
(28) Klayman, D. L.; Scovill, J. P.; Bartosevich, J. F.; Bruce, J. *J. Med. Chem.* **1983**, *26*, 35–39.

separated from the hot solution by filtration, washed with methanol, and dried in vacuo. Yield: 50 mg (39%). Anal. Calcd for $C_{26}H_{24}GaN_{11}O_3S_2 \cdot H_2O$ (M_r = 690.42 g/mol): C, 45.23; H, 3.80; N, 22.32. Found: C, 45.22; H, 3.51; N, 22.20. ESI-MS in MeOH (positive): *m/z* 609, $[Ga(L^H)_2]^+$. IR spectrum in KBr, cm^{-1} (selected bands): 3276 m, 1599 s, 1541 s, 1489 s, 1420 s, 1328 m, 1150 s, 1096 s, 762 s, 698 m, 592 m. UV−vis (MeOH), λ_{max}, nm (ε, M^{-1} cm^{-1}): 230sh (32850), 257 (24810), 270sh (23860), 322 (24570), 430 (31950). ^1H NMR (500.32 MHz, DMSO-d_6): δ 10.46 (s, 2H, NH), 9.66 (s, 2H, pz), 8.96 (d, $^3J_{H,H}$ = 2.8 Hz, 2H, pz), 8.09 (m, 2H, pz), 7.79 (d, $^3J_{H,H}$ = 7.6 Hz, 4H, ph), 7.40 (t, $^3J_{H,H}$ = 7.8 Hz, 4H, ph), 7.13 (t, $^3J_{H,H}$ = 7.6 Hz, 2H, ph), 2.99 (s, 6H, CH_3) ppm. ^{13}C NMR (125.81 MHz, DMSO-d_6): δ 172.3 (C−S), 150.8 (*C*═N), 150.2 (C_{pz}), 147.2 (C_{pz}), 140.3 ($C_{q,ph}$), 139.8 ($C_{q,py}$), 138.9 (C_{pz}), 129.6 (C_{ph}), 124.8 (C_{ph}), 122.5 (C_{ph}), 16.1 (CH_3) ppm. ^{15}N NMR (50.70 MHz, DMSO-d_6): δ 244.7 ($N_{pz,uncoordinated}$) ppm. Crystals suitable for X-ray data collection were obtained from an acetone solution of **1H** saturated with diethyl ether.

[Bis(acetylpyrazine ^{4}*N*-*p*-Nitrophenylthiosemicarbazonato)-*N*,*N*,*S*-gallium(III)]nitrate Monohydrate Methanol Solvate, [Ga-(L^I)$_2$]$NO_3 \cdot H_2O \cdot 0.5CH_3OH$ (1I). To acetylpyrazine ^{4}*N*-*p*-nitrophenylthiosemicarbazone (**HL^I**) (50 mg, 0.158 mmol) in boiling methanol (5 mL) triethylamine (24 μL, 0.173 mmol) and gallium(III) nitrate nonahydrate (33 mg, 0.079 mmol) in methanol (1 mL) were added, and the mixture was stirred under reflux for 3 h. The precipitate was separated from the hot solution by filtration, washed with methanol, and dried in vacuo. Yield: 49 mg (78%). Anal. Calcd for $C_{26}H_{22}GaN_{13}O_7S_2 \cdot H_2O \cdot 0.5CH_3OH$ (M_r = 796.43 g/mol): C, 39.96; H, 3.29; N, 22.86; S, 8.05. Found: C, 40.01; H, 3.12; N, 22.29; S, 7.78. ESI-MS in MeOH (positive): *m/z* 699, $[Ga(L^I)_2]^+$. ESI-MS in MeOH (negative): *m/z* 697, $[Ga(L^I)_2 - 2H]^-$. IR spectrum in KBr, cm^{-1} (selected bands): 3072 m, 1595 m, 1571 m, 1495 s, 1442 s, 1402 m, 1324 s, 1304 s, 1151 m, 1091 s, 853 m, 750 m. UV−vis (MeOH), λ_{max}, nm (ε, M^{-1} cm^{-1}): 219sh (34850), 266 (16800), 309sh (29000), 336 (35740), 415 (42820). ^1H NMR (500.32 MHz, DMSO-d_6): δ 10.92 (s, 2H, NH), 9.76 (d, $^4J_{H,H}$ = 1.3 Hz, 2H, pz), 9.02 (d, $^3J_{H,H}$ = 2.8 Hz, 2H, pz), 8.33 (m, 4H, ph), 8.16 (dd, $^3J_{H,H}$ = 2.8 Hz, $^4J_{H,H}$ = 1.3 Hz, 2H, pz), 8.09 (m, 4H, ph), 3.08 (s, 6H, CH_3) ppm. ^{13}C NMR (125.81 MHz, DMSO-d_6): δ 171.8 (C−S), 154.1 (*C*═N), 150.6 (C_{pz}), 147.3 (C_{pz}), 145.9 ($C_{q,ph}$), 142.5 ($C_{q,ph}$), 139.1 ($C_{q,pz}$), 138.8 (C_{pz}), 125.5 (C_{ph}), 121.2 (C_{ph}), 16.3 (CH_3) ppm.

[Bis(2-acetylpyridine ^{4}*N*-Phenylthiosemicarbazonato)-*N*,*N*,*S*-iron(III)]hexafluorophosphate, [Fe(L^C)$_2$]PF_6 (2C). To 2-acetylpyridine ^{4}*N*-phenylthiosemicarbazone (**HL^C**) (80 mg, 0.296 mmol) in ethanol (7 mL) iron(III) nitrate nonahydrate (67 mg, 0.166 mmol) in ethanol (1 mL) was added, and the reaction mixture was allowed to stir for 5 h at room temperature. Ammonium hexafluorophosphate (100 mg, 0.613 mmol) was added, and the mixture was stirred for further 45 min. The precipitate was filtered off, washed with ethanol, and dried for one week at 50 °C. Yield: 75 mg (68%). Anal. Calcd for $C_{28}H_{26}F_6FeN_8PS_2$ (M_r = 739.50 g/mol): C, 45.48; H, 3.54; N, 15.15. Found: C, 45.66; H, 3.69; N, 15.11. ESI-MS in MeOH (positive): *m/z* 594, $[Fe(L^C)_2]^+$; ESI-MS in MeOH (negative): *m/z* 145, $[PF_6]^-$. IR spectrum in KBr, cm^{-1} (selected bands): 3366 s, 1601 m, 1540 m, 1504 s, 1458 s, 1435 s, 1318 m, 1161 s, 842 vs, 556 m. UV−vis (MeOH), λ_{max}, nm (ε, M^{-1} cm^{-1}): 256 (48440), 388 (33880), 632 (890), 836 (1060).

[Bis(2-acetylpyridine ^{4}*N*-*p*-Nitrophenylthiosemicarbazonato)-*N*,*N*,*S*-iron(III)]nitrate Monohydrate, [Fe(L^D)$_2$]$NO_3 \cdot H_2O$ (2D). To 2-acetylpyridine ^{4}*N*-*p*-nitrophenylthiosemicarbazone (**HL^D**) (150 mg, 0.476 mmol) in boiling methanol (37 mL) iron(III) nitrate nonahydrate (97 mg, 0.240 mmol) in methanol (2 mL) was added, and the reaction mixture allowed to stir for 1 h. The black solid was separated from the hot solution by filtration, washed with methanol, and dried in vacuo. Yield: 115 mg (63%). Anal. Calcd for $C_{28}H_{24}FeN_{11}O_7S_2 \cdot H_2O$ (M_r = 764.55 g/mol): C, 43.99; H, 3.43; N, 20.15. Found: C, 44.34; H, 3.23; N, 19.83. ESI-MS in MeOH (positive): *m/z* 684, $[Fe(L^D)_2]^+$. ESI-MS in MeOH (negative): *m/z* 682, $[Fe(L^D)_2 - 2H]^-$. IR spectrum in KBr, cm^{-1} (selected bands): 3308 m, 3060 m, 1498 s, 1452 s, 1325 s, 1303 s, 1256 s, 1157 s, 1111 s, 854 m, 751 m. UV−vis (MeOH), λ_{max}, nm (ε, M^{-1} cm^{-1}): 237sh (42530), 321sh (27470), 385 (62820), 474sh (7990), 595 (1360), 837 (1220).

[Bis(acetylpyrazine ^{4}*N*-Phenylthiosemicarbazonato)-*N*,*N*,*S*-iron(III)]nitrate Monohydrate, [Fe(L^H)$_2$]$NO_3 \cdot H_2O$ (2H). To acetylpyrazine ^{4}*N*-phenylthiosemicarbazone (**HL^H**) (80 mg, 0.295 mmol) in boiling ethanol (5 mL) iron(III) nitrate nonahydrate (60 mg, 0.149 mmol) in ethanol (2 mL) was added, and the mixture was stirred under reflux for 5 h. The black solid was filtered off from the hot solution, washed with ethanol, and dried in vacuo. Yield: 70 mg (70%). Anal. Calcd for $C_{26}H_{24}FeN_{11}O_3S_2 \cdot H_2O$ (M_r = 676.53 g/mol): C, 46.16; H, 3.87; N, 22.77. Found: C, 46.35; H, 3.74; N, 22.48. ESI-MS in MeOH (positive): *m/z* 596, $[Fe(L^H)_2]^+$. IR spectrum in KBr, cm^{-1} (selected bands): 3245 m, 1597 s, 1547 m, 1428 s, 1342 m, 1148 s, 1094 s, 763 s, 695 m, 585 m. UV−vis (MeOH), λ_{max}, nm (ε, M^{-1} cm^{-1}): 258 (45730), 311sh (22780), 417 (29810), 515sh (6790), 675 (1140), 875 (1010).

[Bis(acetylpyrazine ^{4}*N*-*p*-Nitrophenylthiosemicarbazonato)-*N*,*N*,*S*-iron(III)]nitrate Monohydrate, [Fe(L^I)$_2$]$NO_3 \cdot H_2O$ (2I). To acetylpyrazine ^{4}*N*-*p*-nitrophenylthiosemicarbazone (**HL^I**) (50 mg, 0.158 mmol) in boiling methanol (10 mL), iron(III) nitrate nonahydrate (32 mg, 0.079 mmol) in methanol (2 mL) was added, and the reaction mixture was allowed to stir under reflux for 2 h. The black solid was separated from the hot solution by filtration, washed with methanol, and dried in vacuo. Yield: 37 mg (61%). Anal. Calcd for $C_{26}H_{22}FeN_{13}O_7S_2 \cdot H_2O$ (M_r = 766.53 g/mol): C, 40.74; H, 3.16; N, 23.75. Found: C, 40.77; H, 3.13; N, 23.63. ESI-MS in MeOH (positive): *m/z* 686, $[Fe(L^I)_2]^+$. IR spectrum in KBr, cm^{-1} (selected bands): 3054 m, 1596 m, 1564 m, 1497 s, 1439 s, 1329 s, 1302 s, 1259 m, 1147 s, 1087 s, 850 m, 750 m. UV−vis (MeOH), λ_{max}, nm (ε, M^{-1} cm^{-1}): 226sh (42630), 330 (32320), 399 (47700), 502sh (7440), 662 (1440), 884 (1120).

Crystallographic Structure Determination. X-ray diffraction measurements were performed on a Bruker X8 APEX II CCD-diffractometer. A single crystal of suitable size was protected by Parathone-N oil, attached to a glass fiber, and mounted on a goniometer head at 40 mm from the detector, and 1375, 1594, and 1144 frames were measured, each for 90, 5, and 90 s over 1° scan width. The data were processed using SAINT software.[29] The structures were solved by direct methods and refined by full-matrix least-squares techniques. Non-hydrogen atoms were refined with anisotropic displacement parameters. Hydrogen atoms were placed at calculated positions and refined as riding atoms in the subsequent least-squares model refinements. The isotropic thermal parameters were estimated to be 1.2 times the values of the equivalent isotropic thermal parameters of the atoms to which hydrogens were bound. The following computer programs were used: structure solution, SHELXS-97;[30] refinement, SHELXL-97;[31] molecular diagrams,

(29) *SAINT-Plus*, version 7.06a; *APEX2*; Bruker-Nonius AXS Inc.: Madison, WI, 2004.
(30) Sheldrick, G. M. *SHELXS-97, Program for Crystal Structure Solution*; University Göttingen: Göttingen, Germany, 1997.
(31) Sheldrick, G. M. *SHELXL-97, Program for Crystal Structure Refinement*; University Göttingen: Göttingen, Germany, 1997.

Table 1. Crystal Data and Details of Data Collection for $\mathbf{HL^H}$, $\mathbf{HL^M}$, and **1H**

	$\mathbf{HL^H}$	$\mathbf{HL^M}$	$\mathbf{1H}\cdot H_2O$
empirical formula	$C_{13}H_{13}N_5S$	$C_{10}H_{16}N_4S$	$C_{26}H_{26}GaN_{11}O_4S_2$
fw	271.34	224.33	690.42
space group	$P\bar{1}$	$P2_1/c$	$Pna2_1$
a [Å]	5.7844(14)	5.4716(2)	14.9818(5)
b [Å]	10.036(3)	18.9799(7)	22.0746(7)
c [Å]	11.314(4)	11.8689(4)	8.6006(3)
α [deg]	76.005(12)		
β [deg]	87.021(9)	97.289(2)	
γ [deg]	89.220(9)		
V [Å^3]	636.5(3)	1222.63(8)	2844.37(16)
Z	2	4	4
λ [Å]	0.71073	0.71073	0.71073
ρ_{calcd} [g cm^{-3}]	1.416	1.219	1.612
cryst size [mm^3]	0.16 × 0.01 × 0.01	0.30 × 0.20 × 0.20	0.26 × 0.10 × 0.10
T [K]	100	296	100
μ [mm^{-1}]	0.247	0.241	1.171
R1[a]	0.0440	0.0436	0.0267
wR2[b]	0.0920	0.1362	0.0721
GOF[c]	1.031	1.015	1.055

[a] $R1 = \Sigma||F_o| - |F_c||/\Sigma|F_o|$. [b] $wR2 = (\Sigma[w(F_o^2 - F_c^2)^2]/\Sigma[w(F_o^2)^2])^{1/2}$. [c] $GOF = (\Sigma[w(F_o^2 - F_c^2)^2]/(n-p))^{1/2}$, where n is the number of reflections and p is the total number of parameters refined.

ORTEP;[32] computer, Pentium IV; scattering factors.[33] Crystal data, data collection parameters and structure refinement details for $\mathbf{HL^H}$, $\mathbf{HL^M}$, and **1H** are given in Table 1.

Computational Details. The geometries of the 2-acetylpyridine ^4N,^4N-dimethylthiosemicarbazone ligand $\mathbf{HL^B}$, its deprotonated form $(\mathbf{L^B})^-$, the metal complexes $[Ga(\mathbf{L^B})_2]^+$, $[Fe^{II}(\mathbf{L^B})_2]$, and the reduced form of each of these species were optimized using a combination of the exchange functional of Becke[34a] and the correlation functional of Perdew[34b] (BP86), as implemented in Gaussian 03.[35] The LANL2DZ effective core potentials (ECPs)[36] and the corresponding valence-basis sets were used for the metals, and the 6−31G(d,p) basis sets were used for the other atoms. Vibrational frequencies calculated at this level confirm that all structures are minima on the potential energy surfaces. Improved energies were calculated at the BP86 level together with the same ECPs and valence-basis set on the metal atoms but totally uncontracted and augmented with one set of f functions on Fe,[37] together with the 6−311+G(3d) basis set on the S atoms, and the 6−311+G(d,p) basis sets on the other atoms. Free energies in vacuo were calculated by addition of corrections from unscaled zero-point energy (ZPE), thermal energy, work, and entropy evaluated at the BP86 level at 298.15 K, 1 atm to the improved energies. Standard reduction potentials (SRPs) were calculated according to our previous approach,[38] which was carefully validated for the reduction of 61 ruthenium(III/II) complexes (bearing formal charges from 3+/2+ to 1−/2−) in four solvents and shall be readily transferable to other metal complexes because the metal ion is not solvent-exposed in any of those Ru complexes. The SRP prediction is based on a thermodynamic cycle and involves the calculation of solvation free energies using the Poisson−Boltzmann finite element method,[39] as implemented in Jaguar 7,[40] with dielectric constant of 37.5 representing acetonitrile as the solvent. In the present work, the only difference to our previous SRP calculation approach[38] is the use of the BP86 functional, which leads to excellent agreement with experimental SRPs (see below) and was employed for similar purposes as well.[41a] The overestimation of the contribution of exchange energy by the B3LYP functional[42] is well documented[41b] and may result in the overestimation of the stability of high-multiplicity spin states in iron complexes. A comparison of the relative energies of the electronic states of $[Fe^{II}(\mathbf{L^B})_2]$ and $[Fe^{II}(\mathbf{L^B})_2]^-$ and of the SRPs calculated using the BP86 and B3LYP improved energies is given in the Supporting Information (Tables S1 and S2) and indicates that multireference approaches would be worth considering if permitted by the available computational resources. Other promising methods for this particular purpose include the spectroscopy oriented configuration interaction (SORCI) method and a ligand field theory (LFT)-based approach.[41c] Atomic partial charges at BP86 were calculated using the Mulliken[43a] scheme based on basis functions as implemented in Gaussian, the Hirshfeld[43b] scheme based on electron density as implemented in ADF,[44] and the ESP[43c] scheme of fitting atomic charges to reproduce the electrostatic potential in Jaguar.[40]

Results and Discussion

Synthesis and Characterization. The ligand 2-acetylpyrazine ^4N-phenylthiosemicarbazone ($\mathbf{HL^H}$) (Chart 1) was

(32) Johnson, G. K. *Report ORNL-5138*; Oak Ridge National Laboratory: Oak Ridge, TN, 1976.

(33) *International Tables for X-ray Crystallography*; Kluwer Academic Press: Dodrecht, The Netherlands, 1992; Vol. *C*, Tables 4.2.6.8 and 6.1.1.4.

(34) (a) Becke, A. D. *Phys. Rev. A* **1988**, *38*, 3098–3100. (b) Perdew, J. P. *Phys. Rev. B* **1986**, *33*, 8822–8824.

(35) Frisch, M. J.; Trucks, G. W.; Schlegel, H. B.; Scuseria, G. E.; Robb, M. A.; Cheeseman, J. R.; Montgomery, J. A., Jr.; Vreven, T.; Kudin, K. N.; Burant, J. C.; Millam, J. M.; Iyengar, S. S.; Tomasi, J.; Barone, V.; Mennucci, B.; Cossi, M.; Scalmani, G.; Rega, N.; Petersson, G. A.; Nakatsuji, H.; Hada, M.; Ehara, M.; Toyota, K.; Fukuda, R.; Hasegawa, J.; Ishida, M.; Nakajima, T.; Honda, Y.; Kitao, O.; Nakai, H.; Klene, M.; Li, X.; Knox, J. E.; Hratchian, H. P.; Cross, J. B.; Bakken, V.; Adamo, C.; Jaramillo, J.; Gomperts, R.; Stratmann, R. E.; Yazyev, O.; Austin, A. J.; Cammi, R.; Pomelli, C.; Ochterski, J. W.; Ayala, P. Y.; Morokuma, K.; Voth, G. A.; Salvador, P.; Dannenberg, J. J.; Zakrzewski, V. G.; Dapprich, S.; Daniels, A. D.; Strain, M. C.; Farkas, O.; Malick, D. K.; Rabuck, A. D.; Raghavachari, K.; Foresman, J. B.; Ortiz, J. V.; Cui, Q.; Baboul, A. G.; Clifford, S.; Cioslowski, J.; Stefanov, B. B.; Liu, G.; Liashenko, A.; Piskorz, P.; Komaromi, I.; Martin, R. L.; Fox, D. J.; Keith, T.; Al-Laham, M. A.; Peng, C. Y.; Nanayakkara, A.; Challacombe, M.; Gill, P. M. W.; Johnson, B.; Chen, W.; Wong, M. W.; Gonzalez, C.; Pople, J. A. *Gaussian 03*, revision D.01; Gaussian, Inc.: Wallingford, CT, 2004; www.gaussian.com.

(36) (a) Wadt, W. R.; Hay, P. J. *J. Chem. Phys.* **1985**, *82*, 284–298. (b) Hay, P. J.; Wadt, W. R. *J. Chem. Phys.* **1985**, *82*, 299–310.

(37) Ehlers, A. W.; Böhme, M.; Dapprich, S.; Gobbi, A.; Höllwarth, A.; Jonas, V.; Köhler, K. F.; Stegmann, R.; Veldkamp, A.; Frenking, G. *Chem. Phys. Lett.* **1993**, *208*, 111–114.

(38) Chiorescu, I.; Deubel, D. V.; Arion, V. B.; Keppler, B. K. *J. Chem. Theory Comput.* **2008**, *4*, 499–506.

(39) (a) Tannor, D. J.; Marten, B.; Murphy, R. B.; Friesner, R. A.; Sitkoff, D.; Nicholls, A.; Ringnalda, M. N.; Goddard, W. A., III.; Honig, B. *J. Am. Chem. Soc.* **1994**, *116*, 11875–11882. (b) Marten, B.; Kim, K.; Cortis, C.; Friesner, R. A.; Murphy, R. B.; Ringnalda, M. N.; Sitkoff, D.; Honig, B. *J. Phys. Chem.* **1996**, *100*, 11775–11788.

(40) *Jaguar*, version 7.0; Schrödinger, LCC: New York, 2007; www.schrodinger.com.

(41) (a) Ketterer, N. A.; Fan, H.; Blackmore, K. J.; Yang, X.; Ziller, J. W.; Baik, M.-H.; Heyduk, A. F. *J. Am. Chem. Soc.* **2008**, *130*, 4364–4374. (b) Reiher, M.; Salomon, O.; Hess, B. A. *Theor. Chem. Acc.* **2001**, *107*, 48–55. (c) Fouqueau, A.; Casida, M. E.; Daku, L. M. L.; Hauser, A.; Neese, F. *J. Chem. Phys.* **2005**, *122*, 44110/1–44110/13.

(42) (a) Becke, A. D. *J. Chem. Phys.* **1993**, *98*, 5648–5652. (b) Lee, C.; Yang, W.; Parr, R. G. *Phys. Rev. B* **1988**, *37*, 785–789.

(43) (a) Mulliken, R. S. *J. Chem. Phys.* **1955**, *23*, 1833–1840. (b) Hirshfeld, F. L. *Theor. Chim. Acta* **1977**, *44*, 129–138. (c) Chirlian, L. E.; Miller, M. *J. Comput. Chem.* **1987**, *8*, 894–905.

(44) (a) Te Velde, G.; Bickelhaupt, F. M.; van Gisbergen, S. J. A.; Fonseca Guerra, C.; Baerends, E. J.; Snijders, J. G.; Ziegler, T. *J. Comput. Chem.* **2001**, *22*, 931–967. (b) *ADF 2007.01*; SCM, Theoretical Chemistry, Vrije Universiteit: Amsterdam, The Netherlands, 2007; http://www.scm.com.

synthesized by condensation of ^4N-phenylthiosemicarbazide with acetylpyrazine in boiling ethanol in 73% yield. 2-Acetylpyrazine ^4N-*p*-nitrophenylthiosemicarbazone (**HL^{I}**) was prepared as a pale-yellow powder by reaction of *p*-nitrophenyl isothiocyanate with acetylpyrazine hydrazone in acetonitrile in 75% yield. Acetylpyrazine hydrazone was obtained by reacting acetylpyrazine with an excess hydrazine hydrate as the reagent and solvent. The gallium(III) complex **1C** (Chart 2) was synthesized by reaction of $Ga(NO_3)_3 \cdot 9H_2O$ with 2-acetylpyridine ^4N-phenylthiosemicarbazone in 1:2 molar ratio in ethanol at room temperature, followed by addition of excess NH_4PF_6. Complexes **1D**, **1H**, and **1I** were isolated as nitrates, which precipitated shortly after addition of $Ga(NO_3)_3 \cdot 9H_2O$ to the boiling solution of the corresponding ligand. These complexes show also lower aqueous solubility than the nitrate salts of complexes **1A**−**1C**, **1E**−**1G**, **1J**, and **1K** which because of their good solubility in (m)ethanolic solution were isolated as hexafluorophosphates. The difference in the solubility is also evident for the corresponding iron(III) complexes. Complexes **2D**, **2H**, and **2I** were obtained as nitrate salts by reaction of $Fe(NO_3)_3 \cdot 9H_2O$ with a boiling solution of the ligand, whereas **2C** was isolated as a hexafluorophosphate salt. In contrast to the nonsolvated complexes with secondary amine substituted ligands (**1A**, **1B**, **1E**−**1G**, and iron(III) analogs), microanalytical data for the novel complexes show that they all crystallize with one water molecule. X-ray diffraction studies showed that this water molecule is involved in hydrogen bonding with the NH group of the anilinyl and nitroanilinyl moiety (see below). The presence of crystal water was also confirmed by thermogravimetric analysis (TGA) of complex **1D**, where the loss of water between 40 and 110 °C was observed. A large endothermic peak in the differential thermal analysis (DTA) at 250 °C indicated the pyrolysis of the complex. Taking into account the observed thermal behavior, complex **2C** was dried at 50 °C over one week to give a nonsolvated product.

The UV−vis spectra of the metal-free ligands as well as the gallium(III) complexes are dominated by intraligand transitions associated with the pyridine or pyrazine ring, azomethine, and thione portions of the ligands. The extinction coefficient of the lowest energy band increases dramatically upon coordination of the thiosemicarbazone ligands **HL** to Ga(III) to give $[Ga(L_2)]^+$ concomitant with a small shift of the absorbance maximum (420 → 430 nm for **HL^{H}** → **1H** and 424 → 415 nm for **HL^{I}** → **1I**). The increased extinction coefficient is presumably because of the change in the ligand conjugation caused by the deprotonation of the ligands upon complexation.

The reduced analog of **HL^{B}**, namely **HL^{M}**, was prepared by reduction of an ethanolic solution of methyl 3-[1-(2-pyridyl)ethylidene]hydrazinecarbothioate[28] with $NaBH_4$ and subsequent nucleophilic substitution of the *S*-methyl group by dimethylamine (Chart 1) or by direct reduction of **HL^{B}** with $NaBH_4$ in ethanol. The reduction of the C=N double bond in **HL^{B}** is accompanied by the disappearence of two UV−vis absorption bands with the maxima at 314 and 396 nm as shown in Figure 1. The presence of these two bands

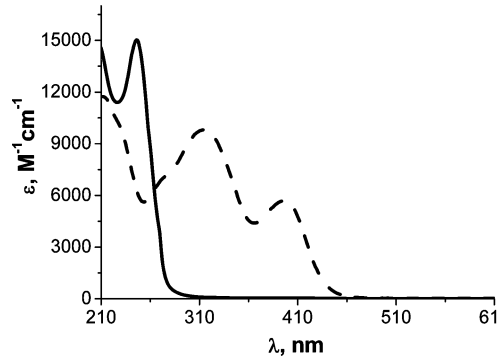

Figure 1. Electronic absorption spectra of ligand **HL^{B}** (dashed line) and its reduced form **HL^{M}** (solid line) in methanol. [**HL^{B}** λ_{max}, nm (ε, M^{-1} cm^{-1}), 231sh (9690), 272sh (6920), 314 (9800), 396 (5680); **HL^{M}** λ_{max}, nm (ε, M^{-1} cm^{-1}), 246 (15030)].

for the π-delocalized thiosemicarbazone chromophore in **HL^{B}** might be explained by the existence of at least two isomers with different electronic structures in solution, as confirmed by ^{1}H NMR measurements in methanol-d_4. In contrast, the ligands **HL^{H}** and **HL^{I}**, which adopt only one isomeric form in solution according to ^{1}H NMR spectra in methanol-d_4, display only one strong absorption band at 326 and 333 nm, respectively. Coordination of the thiosemicarbazone ligands **HL^{H}** and **HL^{I}** to the iron(III) leads to the following changes in their UV−vis spectra: a large increase of the band around 400 nm, appearance of two new bands between 502 and 675 nm (d → π* transition), and around 880 nm the d → d band corresponding to the $^2T_{2g}$ → $^2T_{1g}$ transition of the d^5 low-spin system.[45]

The ^{1}H NMR spectra of the ligands **HL^{H}** and **HL^{I}** recorded in DMSO-d_6 indicate that, in contrast to **HL^{B}**, **HL^{K}**,[24] and other thiosemicarbazones,[46] they exist in solution only as E isomers. Interestingly, the analogous pyridinyl containing ligands **HL^{C}** and **HL^{H}** show small amounts (<10%) of a second isomer with strongly downfield shifted N−H signals at 14.58 and 14.92 ppm, respectively, resulting from intramolecular hydrogen bonding.[25] Like for other reduced thiosemicarbazone ligands,[47] the ^{1}H NMR spectrum of **HL^{M}** indicates the presence of only one isomeric form in solution. Two N−H signals at 8.88 ppm and 5.69 ppm could be observed, where the first one is split into a doublet with a coupling constant of $^3J_{H,H}$ = 5.7 Hz and the second one into a doublet of doublet with $^3J_{H,H}$ = 5.7 Hz and $^3J_{H,H}$ = 3.2 Hz. The coupling constant of 3.2 Hz is also observed for the doublet of quartet of the CH signal at 4.11 ppm, with the quartet splitting ($^3J_{H,H}$ = 6.6 Hz) originating from the coupling with the C*H*$_3$CH−N methyl group at 1.30 ppm (d, $^3J_{H,H}$ = 6.6 Hz). Consequently, the signal at 8.88 ppm can be attributed to the S=CN*H* proton and that at 5.69 ppm to the CHN*H* proton. A 2D ^{1}H−^{15}N HSQC NMR spectrum shows one resonance at 116.7 ppm associated to the proton signal at 8.88 ppm and a second resonance at 76.8 ppm coupled with the proton at 5.69 ppm. The long-range ^{1}H−^{15}N

(45) Sreekanth, A.; Fun, H.-K.; Kurup, M. R. P. *J. Mol. Struct.* **2005**, *737*, 61–67.
(46) Easmon, J.; Heinisch, G.; Holzer, W. *Heterocycles* **1989**, *29*, 1399–1408.
(47) Easmon, J.; Heinisch, G.; Holzer, W. *Sci. Pharm.* **1993**, *61*, 3–10.

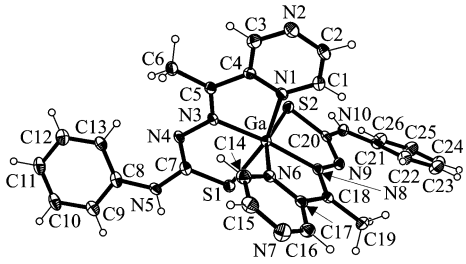

Figure 2. ORTEP plot with thermal ellipsoids at 50% probability level for complex cation $[Ga(\mathbf{L^H})_2]^+$ in **1H** with atom labeling scheme. Selected bond distances (Å) and angles (deg): C5−N3 = 1.292(3), C18−N8 = 1.297(4), N3−N4 = 1.367(3), N8−N9 = 1.364(3), N4−C7 = 1.320(4), N9−C20 = 1.325(4), C7−S1 = 1.734(3), C20−S2 = 1.743(3), C7−N5 = 1.356(4), C20−N10 = 1.346(3); N1−Ga−N3 = 76.98(9), N6−Ga−N8 = 76.16(9), N3−Ga−S1 = 83.34(6), N8−Ga−S2 = 83.72(7).

HMBC spectrum shows that the two N−H groups couple with each other and, in addition, that the signal at 116.7 ppm ($^1J_{N,H}$ = 98 Hz) couples with the tertiary CH signal δ = 4.11 ppm, whereas the nitrogen resonance at 76.8 ppm ($^1J_{N,H}$ = 78 Hz) exhibits a cross peak with the CH_3 group resonance at 1.30 ppm. All this confirms the above-mentioned assignments. In addition, three pyridine protons give a cross peak with the ^{15}N resonance at 291.2 ppm, which can be ascribed to the pyridine nitrogen.

In contrast to some of the metal-free ligands, the ^{1}H NMR spectra of the gallium complexes **1C**, **1D**, **1H**, and **1I** show only one set of signals because of the stabilization of the ligand configuration upon coordination to the metal and the equivalence of both ligands bound to gallium(III) in solution. The most remarkable difference between the ^{1}H NMR spectra of the gallium complexes and those of the metal-free ligands is the absence of one of the N−H signals, indicating deprotonation of the ligands upon complexation. Because it was difficult to distinguish between the two quaternary carbon atoms of the pyridine and pyrazine ring, respectively, and the carbon of the adjacent C=N double bond, complex **1H** was studied by multinuclear (^{1}H, ^{13}C, and ^{15}N) one- and two-dimensional NMR spectroscopy. Exact assignment of the quaternary carbon atoms was necessary for the correlation of the ^{13}C NMR chemical shifts with the redox potentials (see Figure 9). In general, the ^{13}C NMR chemical shifts of the C=N bond of the gallium complexes occur at lower field than the quaternary carbon atoms of the heterocycle (for detailed discussion see Supporting Information).

Crystal Structures. $[Ga(\mathbf{L^H})_2]NO_3 \cdot H_2O$ (**1H**) crystallized in the orthorhombic space group $Pna2_1$, while $\mathbf{HL^H}$ crystallized in the triclinic centrosymmetric space group $P\bar{1}$. The structure of the complex cation is shown in Figure 2, and the molecular structure of the metal-free ligand $\mathbf{HL^H}$ is shown in Figure 3. Selected bond distances (Å) and angles (deg) are quoted in the legends to the Figures 2 and 3. The asymmetric unit of **1H** consists of a distorted octahedral $[Ga(\mathbf{L^H})_2]^+$ complex cation, a counteranion NO_3^-, and a cocrystallized water molecule. Each ligand is monodeprotonated and coordinates to gallium via the pyrazine nitrogen atom [Ga−N1 = 2.142(2) Å, Ga−N6 = 2.155(2) Å], an azomethine nitrogen [Ga−N3 = 2.033(2) Å, Ga−N8 = 2.044(2) Å], and a sulfur donor atom [Ga−S1 = 2.3266(8) Å, Ga−S2 = 2.3249(8) Å], forming two five-membered

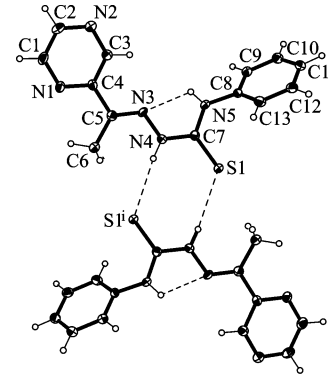

Figure 3. Centrosymmetric dimeric associate of $\mathbf{HL^H}$, emphasizing the intra- and intermolecular hydrogen-bonding interactions; symmetry code i: $-x + 3, -y + 1, -z + 1$. Selected bond distances (Å) and angles (deg): C4−C5 = 1.481(4), C5−N3 = 1.284(3), N3−N4 = 1.367(3), N4−C7 = 1.366(3), C7−S1 = 1.677(3), C7−N5 = 1.335(3), N5−C8 = 1.425(3); $\Theta_{C3-C4-C5-N3}$ = 12.3(4), $\Theta_{N3-N4-C7-S1}$ = 174.06(18).

chelate rings, correspondingly. Both coordinated ligands are essentially planar, with exception of the phenyl group at the terminal nitrogen atom of the thiosemicarbazide moiety. The deviation from planarity of the phenyl ring in each coordinated ligand can be described by torsion angles $\Theta_{C13-C8-N5-C7}$ and $\Theta_{C20-N10-C21-C22}$ of 8.2(5)° and −21.5(4)°, respectively. The bond distances C7−S1 of 1.734(3) Å and C20−S2 of 1.743(3) Å are comparable to those reported for $[Ga(\mathbf{L^G})_2][PF_6]$ ($\mathbf{HL^G}$ = acetylpyrazine ^4N,^4N-dimethylthiosemicarbazone)[23] at 1.754(2) and 1.745(2) Å and are significantly longer than that of the metal free ligand $\mathbf{HL^H}$ at 1.677(3) Å. Of note are the angles N1−Ga−S1 at 159.55(7)° and N6−Ga−S2 at 156.90(7)°, which deviate markedly from the ideal value of 180°. The reason might be some repulsion between S1 and S2 (S1···S2 = 3.572 Å). The molecules of **1H** are involved into a network of intermolecular hydrogen bonds, with the NH groups of both thiosemicarbazone ligands and the water molecule acting as proton donors and the oxygens of the water and the nitrate counterion acting as proton acceptor (N10−H···O3···H−O4···H−N5).

The crystal structure of the ligand $\mathbf{HL^H}$ has an essentially nonplanar conformation (Figure 3), which differs markedly from that imposed by coordination. The phenyl ring C8−C13 and the pyrazine ring form dihedral angles of 54.2 and 164.7° with the central mean plane through N3, N4, C7, and N5 atoms of the thiosemicarbazide residue. Two rotations, one about C4−C5 bond and another about N4−C7 bond by ∼180° in the metal-free ligand are necessary to achieve the conformation adopted by both ligands in $[Ga(\mathbf{L^H})_2]^+$. The molecules of $\mathbf{HL^H}$ are associated in centrosymmetric dimers via hydrogen bonding interactions of the type N4−H···S1 ($-x + 3, -y + 1, -z + 1$) [N4−H = 0.88 Å, H···S1 = 2.691 Å, N4···S1 = 3.568 Å, N4−H···S1 = 174.08°]. Although it is weak, the intramolecular H bond N5−H···N3 [N5−H = 0.794 Å, H···N3 = 2.159 Å, N5···N3 = 2.585 Å, N5−H···N3 = 113.90°] is also of note.

The result of X-ray diffraction study for $\mathbf{HL^M}$ is displayed in Figure 4. The reduction of the azomethine bond is evidenced by the sp^3-hybridized atoms C6 (tetrahedral configuration) and N2 and by the lengths of the bonds

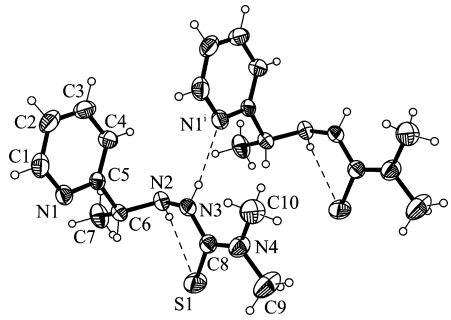

Figure 4. ORTEP plot of a fragment of the crystal structure of $\mathbf{HL^M}$ with thermal ellipsoids at 40% probability level, showing the intra- and intermolecular hydrogen-bonding interactions; symmetry code i: $x-1, y, z$. Selected bond distances (Å) and angles (deg): C5−C6 = 1.503(3), C6−N2 = 1.471(2), N2−N3 = 1.418(2), N3−C8 = 1.359(3), C8−S1 = 1.685(2), C8−N4 = 1.340(3) Å; $\Theta_{N1-C5-C6-N2} = -151.70(16)$, $\Theta_{C5-C6-N2-N3} = -75.1(2)$, $\Theta_{N2-N3-C8-S1} = -10.6(3)$.

involving these atoms. The overall conformation of the molecule is strongly distorted. The dihedral angle between the pyridine ring and the plane through the N3, C8, N4, and S1 atoms of the thiosemicarbazide moiety is 85.9°. The molecules of $\mathbf{HL^M}$ are involved in intramolecular hydrogen bonding interactions of the type N2−H···S1 [N2−H = 0.881 Å, H···S1 = 2.529 Å, N2···S1 = 2.950 Å, N2−H−S1 = 110.10°] and in a strong intermolecular H bond N3−H···N1 ($x-1, y, z$) [N3−H = 0.834 Å, H···N3 = 2.218 Å, N3···N1 = 3.041 Å, N3−H···N1 = 169.00°]. A search at CSD[48] did not show any deposited X-ray diffraction data for reduced thiosemicarbazones.

Electrochemical Studies. Ligand-Centered Reduction. The electrochemical data for the metal complexes and ligands under study are summarized in Tables 2 and S3 (Supporting Information), respectively, and their electrochemical behavior is shown in Scheme 1. In general, the complexes show several redox waves attributable to the reduction of the noninnocent thiosemicarbazone ligands at lower potentials (<−0.4 V vs NHE) than the metal-centered redox waves for the iron and ruthenium complexes (>0 V vs NHE; see below). The cyclic voltammograms of 0.20 M [n-Bu_4N][BF_4]/CH_3CN solutions of the gallium thiosemicarbazonate complexes **1A**−**1I** display two consecutive reversible one-electron (as confirmed by controlled potential electrolysis of **1B**) redox waves with ${}^{ox}i_p/{}^{red}i_p = 1.0$ at $v > 50$ mV/s with $\Delta E_p = 60-70$ mV at 0.20 V/s (Scheme 1a, Figure 5). The redox potential of the first ligand reduction (wave ${}^{I}L^{red}$) occurs between −0.38 and −0.96 V, and the second (wave ${}^{II}L^{red}$) between −0.62 and −1.25 V vs NHE depending on the ligand identity (Table 2). As expected, complex **1A** with the 2-pyridinyl and 4-pyrrolidinyl substituents at the thiosemicarbazone ligands shows the most negative redox potentials, whereas complex **1I** with the more electron-withdrawing moieties nitroanilinyl and 2-pyrazinyl (the latter being weaker σ-donor and stronger π-acceptor than the 2-pyridinyl moiety) has the most positive redox potential for the ligand-centered reductions.

After these two consecutive reversible reduction processes a third irreversible redox wave ${}^{III}L^{red}$ is observed for the pyridinyl complexes **1A**−**1C** between −1.63 and −1.81 V vs. NHE, whereas wave ${}^{III}L^{red}$ is a reversible one-electron reduction process at −1.35 and −1.56 V vs NHE for the pyrazinyl containing complexes **1E**−**1H** and is followed by a fourth partially quasi-reversible one-electron reduction wave, ${}^{IV}L^{red}$, at approximately −1.80 V vs NHE (ΔE_p = 100−150 mV) (Figure 6a). For complex **1H**, this fourth reduction wave is irreversible because it overlaps with a further wave at approximately −1.95 V vs NHE. Waves ${}^{III}L^{red}$ and ${}^{IV}L^{red}$ were not detected for **1D** and **1I**, both containing a nitro-group attached to the thiosemicarbazone ligand, but instead a quasi-reversible ($\Delta E_p = 90-100$ mV) reduction of the NO_2 group[49] at $E_{1/2} = -1.04$ and −1.01 V vs NHE was observed, respectively. Complexes with nitro-derivatives are scarcely soluble in CH_3CN and were therefore measured in 0.20 M [n-Bu_4N][BF_4]/DMF. However, no variations in redox properties/potentials of the complexes

Table 2. Summary of the Electrochemical Data[a] for the Metal Complexes

	gallium complexes		
	$E_{1/2}/{}^{I}L^{red}$	$E_{1/2}/{}^{II}L^{red}$	$E_{1/2}/{}^{III}L^{red}$
1A	−0.96	−1.25	−1.81[c,e]
1B	−0.93	−1.22	−1.77[c,e]
1C	−0.79	−1.05	−1.63[c]
1D[b]	−0.70[c]	NA[f]	NA[f]
1E	−0.60	−0.88	−1.56
1F	−0.58	−0.84	−1.49
1G	−0.58	−0.85	−1.51
1H	−0.46	−0.72	−1.35
1I[b]	−0.38[d]	−0.62[d]	NA[f]
1J	−1.03	−1.34	−2.04[c]
1K	−0.94	−1.22	−1.73[c,e]

	iron complexes				
	$E_{1/2}/{}^{C}Fe^{red}$	$E_{1/2}/{}^{A}Fe^{red}$	$E_{1/2}/{}^{I}L^{red}$	$E_{1/2}/{}^{II}L^{red}$	$E_p/{}^{III}L^{red}$
2A	0.06		−1.62[d]	−2.01[c,g]	−2.01[c,g]
2B	0.08		−1.61[d]	−1.99[c,g]	−1.99[c,g]
2C	0.18		−1.44[d]	−1.72[d]	−2.15[c,e]
2D[b]	0.27		NA[f]	NA[f]	NA[f]
2E	0.32		−1.23	−1.65	−2.12[c,e]
2F	0.32		−1.21	−1.64	−2.09[c,e]
2G	0.34		−1.22	−1.64	−2.13[c,e]
2H	0.43		−1.08	−1.47	−1.97[c,e]
2I[b]	0.51		NA[f]	NA[f]	NA[f]
2′A	0.06	0.30	−1.60[c]		
2′B	0.08	0.30	−1.61[d]		
2′E	0.31[g]	0.31[g]	−1.20[c]		
2′F	0.31[g]	0.31[g]	−1.21[d]		
2′G	0.32[g]	0.32[g]	−1.22[d]		

	ruthenium complex				
	$E_{1/2}/Ru^{III/II}$	$E_{1/2}/Ru^{IV/III}$	$E_{1/2}/{}^{I}L^{red}$	$E_p/{}^{II}L^{red}$	$E_p/{}^{III}L^{red}$
3B	+0.21	+1.27	−1.56	−2.00[c,g]	−2.00[c,e,g]

[a] Potentials in $V \pm 0.01$ vs NHE in 0.20 M [n-Bu_4N][BF_4]/CH_3CN. [b] Measured in 0.20 M [n-Bu_4N][BF_4]/DMF. [c] For the irreversible wave, the E_p values are given. [d] ${}^{ox}i_p/{}^{red}i_p$ between 0.6 and 0.8 at 0.2 V/s. [e] Two- or multielectron process (see text). [f] For complexes with nitro-containing ligands, the reduction of this group at approximately −1.0 V vs NHE prevented the detection of further ligand-centered redox waves (see text). [g] Could not be detected as separate waves.

(48) *Cambridge Structure Database*, version 5.29; Cambridge Crystallographic Data Centre: Cambridge, U.K., 2007.

(49) Geske, D. H.; Ragle, J. L.; Bambenek, M. A.; Balch, A. L. *J. Am. Chem. Soc.* **1964**, *86*, 987–1002.

Scheme 1. Overview of the Electrochemical Behavior of the Studied Ga (a), Fe (b), and Ru (c) Complexes

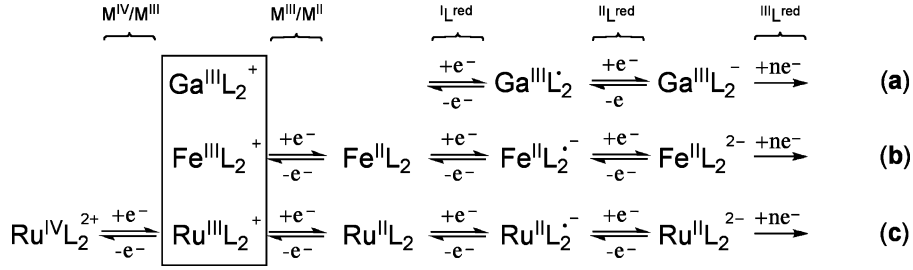

have been observed in DMF or CH_3CN electrolyte solutions as established for complex **2D**.

The influence of the chalcogen atom X of the chalcogensemicarbazone ligands (Chart 1) on the redox potential was studied with complexes **1B**, **1J**, and **1K**, which contain a sulfur, oxygen, or selenium atom, respectively. Complex **1J** (X = O) displays the lowest reduction potentials at −1.03 and −1.34 V vs NHE for $^{I}L^{red}$ and $^{II}L^{red}$, respectively, whereas **1K** (X = Se) and **1B** (X = S) have similar redox potentials at −0.93 to −0.94 and −1.22 V vs NHE for the corresponding redox waves. Thio- and selenosemicarbazone ligands are known to have comparable NMR spectra,[50] and the gallium complexes **1B** and **1K** also possess similar ^{1}H and ^{13}C NMR chemical shifts with the largest deviation in the ^{13}C NMR spectra of the C−X resonance (detected at 176.1 and 173.8 ppm, respectively).[23,24] Complex **1J** shows a considerably different spectrum with the C−X resonance at 167.1 ppm and strong upfield shifts for both carbon resonances at the $CH_3C{=}N$ moiety (**1B** 14.9, 149.0 ppm; **1K** 15.6, 147.4 ppm; **1J** 12.6, 139.3 ppm); in accordance with the lower redox potential of complex **1J** (see below).

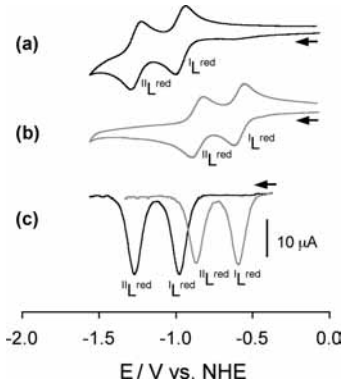

Figure 5. Cyclic voltammograms of (a) **1A** and (b) **1F** in CH_3CN containing 0.20 M [n-Bu_4N][BF_4] at a scan rate of 0.20 V s^{-1} using a platinum working electrode. Square wave voltammograms (SWVs); (c) of 1.0 mM **1A** (black line) and **1F** (gray line) electrolyte solutions were measured with 2 mV step height, 25 mV pulse, and 100 Hz frequency. The solid line on the bottom right refers to the current (10 μA) for a−c. For the assignment of waves, see text.

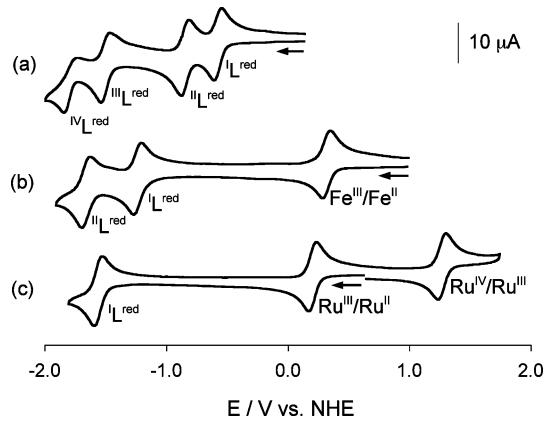

Figure 6. Cyclic voltammograms of **1G** (a), and **2E** (b), and **3B** (c) in CH_3CN containing 0.20 M [n-Bu_4N][BF_4] at a scan rate of 0.20 V s^{-1} using a glassy carbon working electrode, displaying the ligand (L^{red}), the Fe^{III}/Fe^{II} ($^{C}Fe^{red}$), and the Ru^{III}/Ru^{II} and Ru^{IV}/Ru^{III} redox couples.

The ligand-centered reduction of the iron complexes **2A**−**2I** (for $Fe^{III} \rightarrow Fe^{II}$ process see below) is similar to that for the gallium analogs, although the corresponding redox potentials $^{I}L^{red}$ and $^{II}L^{red}$ are considerably more negative between −1.08 and −1.62 V, and −1.47 and −2.01 V vs NHE, respectively (Scheme 1b, Figure 6b, Table 2). In the case of **2A** and **2B** the wave $^{II}L^{red}$ at −2.01 and −1.99 V vs NHE overlaps with $^{III}L^{red}$ resulting in two indistinguishable redox waves. Complexes **2C**−**2H** are reduced at $^{III}L^{red}$ between −1.97 and −2.15, close to the solvent cutoff potential. The lower redox potentials of the iron(II) compared to the gallium(III) complexes are in line with the calculated higher LUMO energy level (see below) and the neutral charge of the iron(II) complexes (compared to the positively charged gallium complexes). For the nitro group containing complexes **2D** and **2I** only one ligand-centered irreversible reduction wave at −0.97 and −0.93 V vs NHE was detected, which can be attributed to the reduction of the nitro group. This is only slightly shifted to more positive potential compared to that in the analogous gallium complexes. The presence of the tetrachloridoferrate counteranion in **2′A**−**2′G** prevented the accurate detection of the second reduction wave $^{II}L^{red}$ in these complexes, because the counteranion reacts readily with the ligand radical formed upon reduction at $^{I}L^{red}$.

The ruthenium complex **3B** shows the first ligand reduction at $E_{1/2}$ = −1.56 V vs NHE (Scheme 1c, Figure 6c), whereas $^{II}L^{red}$, like for the pyridine containing iron complexes **2A** and **2B**, overlaps with $^{III}L^{red}$ resulting in an irreversible reduction wave at −2.00 V (see Supporting Information, Figure S1).

Increasing electron donor properties of substituents are known to increase the effective negative net charge on the corresponding molecules and result usually in a decrease of

(50) Castle, T. C.; Maurer, R. I.; Sowrey, F. E.; Went, M. J.; Reynolds, C. A.; McInnes, E. J. L.; Blower, P. J. *J. Am. Chem. Soc.* **2003**, *125*, 10040–10049.

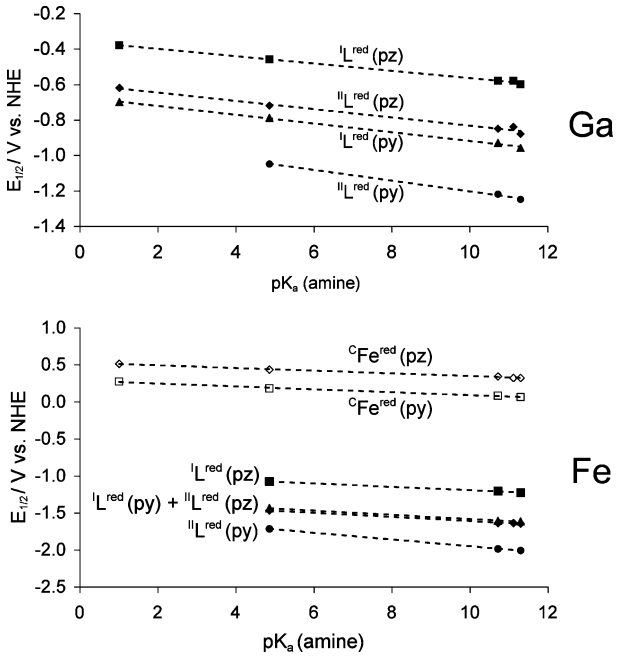

Figure 7. Plot of pK_a values of attached amine moieties on thiosemicarbazone ligands vs ligand- and metal-centered $E_{1/2}$ values for the gallium (**1A**−**1I**, top) and iron (**2A**−**2I**, bottom) complexes. For the complexes **1D**, **2D**, and **2I**, the reduction of the nitro group prevented the detection of $^{I}L^{red}$ and/or $^{II}L^{red}$. $^{C}Fe^{red}$ = Fe^{III}/Fe^{II} redox couple of complex cation; L^{red} = ligand-centered reduction; thiosemicarbazonate complexes with pyrazine (pz) or pyridine (py) moieties are shown separately. Linear equations for gallium complexes: $^{I}L^{red}$ (pz) $E_{1/2}$ (V) = −0.359 − 0.0206·pK_a (r = 0.996); $^{II}L^{red}$ (pz) $E_{1/2}$ (V) = −0.600 − 0.0233·pK_a (r = 0.985); $^{I}L^{red}$ (py) $E_{1/2}$ (V) = −0.673 − 0.0247·pK_a (r = 0.997); $^{II}L^{red}$ (py) $E_{1/2}$ (V) = −0.902 − 0.0302·pK_a (r = 0.997). Linear equations for iron complexes: Fe^{III}/Fe^{II} (pz) $E_{1/2}$ (V) = 0.524 −0.018·pK_a (r = 0.995); Fe^{III}/Fe^{II} (py) $E_{1/2}$ (V) = 0.285 − 0.0197·pK_a (r = 0.995); $^{I}L^{red}$ (pz) $E_{1/2}$ (V) = −0.969 − 0.0227·pK_a (r = 0.998); $^{I}L^{red}$ (py) $E_{1/2}$ (V) = −1.302 − 0.0284·pK_a (r = 0.999); $^{II}L^{red}$ (pz) $E_{1/2}$ (V) = −1.334 − 0.0279·pK_a (r = 0.997); $^{II}L^{red}$ (py) $E_{1/2}$ (V) = −1.499 − 0.0455·pK_a (r = 0.999).

their redox potentials. Plotting the pK_a values of the attached amine moieties [pyrrolidine (11.31), piperidine (11.12), dimethylamine (10.73), aniline (4.87) and *p*-nitroaniline (1.02)][51] versus $E_{1/2}$ results in a linear relationship (Figure 7). The resultant linear equations (see caption of Figure 7) and the pK_a values of the attached amine moieties can be used to predict the redox potentials of novel 2-acetylpyridine(pyrazine) thiosemicarbazone gallium(III) and iron(III) complexes in CH_3CN solution. The increased redox potential of complexes containing a pyrazine (**1E**−**1I**, **2E**−**2I**) instead of a pyridine (**1A**−**1D**, **2A**−**2D**) moiety can also be rationalized by the increased net donor properties of the latter [E_L(pyridine) = 0.25 V, E_L(pyrazine) = 0.33][9] and the different pK_a values [pK_a(pyrazine) = 0.65, pK_a(pyridine) = 5.23], respectively.[51]

The metal-free thiosemicarbazone ligands $\mathbf{HL^A}$–$\mathbf{HL^I}$ exhibit an irreversible reduction response at −1.01 to −1.47 V vs NHE (Table S3, Supporting Information). The second reduction wave could only be observed occasionally and was hardly reproducible, indicating the instability of the radical formed after the first reduction process. For the *p*-nitrophenyl ligands $\mathbf{HL^D}$ and $\mathbf{HL^I}$, a quasi-reversible nitro reduction wave was detected at −1.04 and −1.03 V vs NHE, respectively.[49] In agreement with the peripheral position of the nitro group in the ligands, their reduction potentials are only slightly more negative than those of the corresponding ligands in the gallium and iron complexes. In addition, an irreversible prewave was observed at E_p = −0.82 and −0.80 V vs NHE, respectively, which was also reported for *o*-nitrotoluene and *m*-nitrotoluene in aprotic solvents.[52] In contrast to the ligand-centered reduction in the metal complexes where both ligands are forced to adopt the same configuration, the metal-free ligands are present as different isomers in solution, therefore showing no conclusive correlation between the E_p and pK_a values of the amine moieties of the ligand. In particular, for ligand $\mathbf{HL^B}$ three different isomers were found in DMSO solution,[24] two of them with strong intramolecular hydrogen bonds, whereas ligand $\mathbf{HL^H}$ in the same solvent is present as one isomer (see NMR data). The metal-ion stabilizes the reduced ligand radicals preventing their decomposition on the time-scale of cyclic voltammetry and allowing for the observation of two or three reversible ligand-centered redox waves upon coordination. The gallium-complexes are reduced at ∼0.3−0.8 V more positive redox potential than the uncoordinated ligands, whereas the same ligand-centered reductions in the iron(II) and ruthenium(II) complexes occur at ∼0.0−0.4 V more negative redox potentials than in the metal-free thiosemicarbazones. Therefore complexation to different metal ions strongly influences the ligand-centered redox potentials, offering the possibility to specifically shift them into the physiologically accessible range.

Metal-Centered Redox Processes. The cyclic voltammograms of the iron complexes **2A**−**2I** (Figure 8a, Table 2) display one reversible single-electron reduction wave, $^{C}Fe^{red}$, at 0.06 to 0.51 V vs NHE, which is assigned to the $Fe^{III} \rightarrow Fe^{II}$ process of the cationic complex ($^{ox}i_p/^{red}i_p$ = 1.0 for υ > 0.05 V/s with ΔE_p = 0.60−0.70 at 0.2 V/s). As observed for the ligand-centered redox behavior, an increasing net electron-donor character of the ligands (expressed by their basicity; pK_a values of substituents) correlates with a decrease in redox potential of the iron-centered redox couples (Figure 7). Whereas complexes **2A**−**2I** showed only one reduction wave (Figure 8a), the analogous complexes **2′A**−**2′G** displayed a second wave at 0.31 ± 0.01 V vs NHE, which is attributed to the reduction of the tetrachloridoferrate anion, $^{A}Fe^{red}$ (Figure 8b). Wave $^{A}Fe^{red}$ overlaps in **2′E**−**2′G** with the reduction wave of the complex cation, $^{C}Fe^{red}$, and could not be resolved by cyclic or square wave voltammetry, indicating that a set of two anionic tridentate ligands $\mathbf{HL^E}$−$\mathbf{HL^G}$ acts as a net electron-donor as strong as four tetrahedrally coordinated chlorido ligands. The current height of the Fe^{III}/Fe^{II} redox couple in **2′E**−**2′G** (same concentration and experimental conditions) was approximately 2-fold compared to that of **2E**−**2G**, as confirmed by cyclic and square wave voltammetry (Figure 8). Therefore, the unresolved wave in **2′E**−**2′G** arises from an overlap of the Fe^{III}/Fe^{II} waves of the cationic iron complex and the tetrachlo-

(51) *CRC Handbook of Chemistry and Physics*; Lide, D. R., Ed.; CRC Press: Boca Raton, FL, 2004.

(52) Nunez-Vergara, L. J.; Bonta, M.; Navarrete-Encina, P. A.; Squella, J. A. *Electrochim. Acta* **2001**, *46*, 4289–4300.

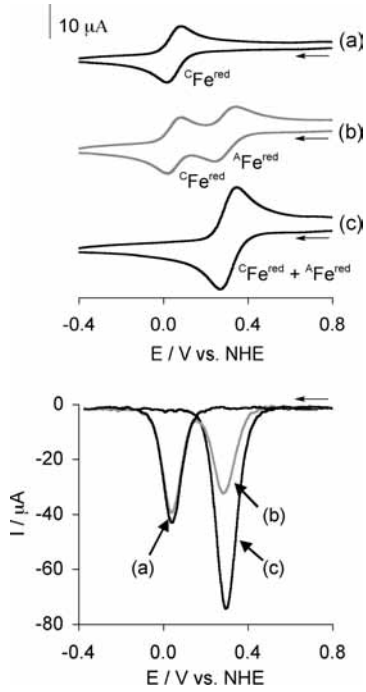

Figure 8. Cyclic voltammograms (top, 0.20 V s^{-1}) and square wave voltammograms (bottom, 2 mV step height, 25 mV pulse, 100 Hz frequency) of (a) **2A** (black), (b) **2′A** (gray), (c) **2′E** (black) in 0.20 M [*n*-Bu_4N][BF_4]/CH_3CN by using a platinum working electrode. $^{C}Fe^{red}$ indicates the metal-centered reduction of the cathodic complex, and $^{A}Fe^{red}$ the reduction of the $[FeCl_4]^-$ counteranion.

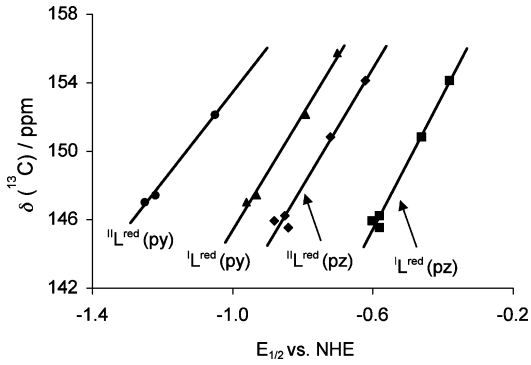

Figure 9. Plot of $\delta(^{13}C{=}N)$ of the $CH_3C{=}N$ moiety vs $E_{1/2}$ of complexes **1A**−**1H** (pz = pyrazine; py = pyridine). Linear equations: $^{I}L^{red}$ (pz) $E_{1/2}$ (V) = (δ − 168.96)/39.35 (r = 0.987); $^{II}L^{red}$ (pz) $E_{1/2}$ (V) = (δ − 175.32)/34.29 (r = 0.972); $^{I}L^{red}$ (py) $E_{1/2}$ (V) = (δ − 179.19)/33.89 (r = 0.993); $^{II}L^{red}$ (py) $E_{1/2}$ (V) = (δ − 179.61)/26.23 (r = 0.995).

ridoferrate anion indicating the two-electron nature of this reduction wave (Figure 8). The presence of two overlapped one-electron processes in **2′E**−**2′G** was confirmed by controlled potential electrolysis of **2′F** at 0.14 V vs NHE.

The ruthenium(III) complex shows two reversible metal-centered redox waves with the first one at +0.21 V for the $Ru^{III} \rightarrow Ru^{II}$ redox couple and the second at +1.27 vs NHE attributable to the $Ru^{III} \rightarrow Ru^{IV}$ redox process (Figure 6c). The 1.06 V difference for the $Ru^{III} \rightarrow Ru^{II}$ and $Ru^{III} \rightarrow Ru^{IV}$ redox couples is small compared to the commonly observed separation of these two redox waves of ∼1.6 V for octahedral ruthenium complexes in nonaqueous solvents.[53] However, this difference can be explained by the distortion of the octahedral geometry resulted from coordination of the tridentate thiosemicarbazonate ligands to ruthenium, which makes direct comparisons with other sterically nonconstrained complexes difficult.

Location of Ligand-Centered Reduction Site. Most of the literature dealing with electrochemical properties of α-*N*-heterocyclic thiosemicarbazone complexes is exclusively focused on the metal-centered redox reactions,[54−57] neglecting the ligand-centered redox processes. If reductions are described that are associated with the ligand, the position where reduction takes place in the thiosemicarbazone moiety is either undefined[58−60] or changes between the thione portion[61] and the azomethine part,[62] whereas no further studies are reported to support these assumptions. Detailed investigations on the reduction pathway were performed for the metal-free 2-formylpyridine thiosemicarbazone in methanol.[63] The data showed that the ligand is first protonated at the azomethine nitrogen then cleaved at the N−N bond, forming thiourea and the 2-pyridinemethaniminium ion, which is then further reduced to protonated 2-picolylamine. Two other reduction mechanisms were excluded in that study, namely, the reduction at the pyridine ring resulting in dihydropyridine and the formation of the thiol by reduction of the C=S double bond. The direct reduction of the azomethine bond was already reported for the same ligand in water 20 years ago.[64] There is only one publication dealing with the metal ion influence on the redox potentials of a thiosemicarbazone ligand.[65] Although the reference electrode was not specified, making a quantitative comparison impossible, the reported redox potentials of the perchlorate salt of the iron(III) complex **2B** and the ligand $\mathbf{HL^B}$ appeared at considerably different values for all reduction waves than observed in the present study. To the best of our knowledge,

(53) Reisner, E.; Arion, V. B.; Guedes da Silva, M. F. C.; Lichtenecker, R.; Eichinger, A.; Keppler, B. K.; Kukushkin, V. Yu.; Pombeiro, A. J. L. *Inorg. Chem.* **2004**, *43*, 7083–7093.

(54) Bindu, P.; Kurup, M. R. P.; Satyakeerty, T. R. *Polyhedron* **1998**, *18*, 321–331.

(55) Prabhakaran, R.; Renukadevi, S. V.; Karvembu, R.; Huang, R.; Mautz, J.; Huttner, G.; Subashkumar, R.; Natarajan, K. *Eur. J. Med. Chem.* **2008**, *43*, 268–273.

(56) Sengupta, P.; Dinda, R.; Ghosh, S.; Sheldrick, W. S. *Polyhedron* **2003**, *22*, 447–453.

(57) Ainscough, E. W.; Brodie, A. M.; Denny, W. A.; Finlay, G. J.; Ranford, J. D. *J. Inorg. Biochem.* **1998**, *70*, 175–185.

(58) Kovala-Demertzi, D.; Domopoulou, A.; Demertzis, M. A.; Papageorgiou, A.; West, D. X. *Polyhedron* **1997**, *16*, 3625–3633.

(59) Costa, R. F. F.; Rebolledo, A. P.; Matencio, T.; Calado, H. D. R.; Ardisson, J. D.; Cortes, M. E.; Rodrigues, B. L.; Beraldo, H. *J. Coord. Chem.* **2005**, *58*, 1307–1319.

(60) Graminha, A. E.; Vilhena, F. S.; Batista, A. A.; Louro, S. R. W.; Ziolli, R. L.; Teixeira, L. R.; Beraldo, H. *Polyhedron* **2008**, *27*, 547–551.

(61) Aguirre, M.; Borras, J.; Castineiras, A.; Garcia-Monteagudo, J. M.; Garcia-Santos, I.; Niclos, J.; West, D. X. *Eur. J. Inorg. Chem.* **2006**, 1231–1244.

(62) Chattopadhyay, S. K.; Chattopadhyay, D.; Banerjee, T.; Kuroda, R.; Ghosh, S. *Polyhedron* **1997**, *16*, 1925–1930.

(63) Pessôa, M. M. B.; Andrade, G. F. S.; dos Santos, M. R.; Temperini, M. L. A. *J. Electroanal. Chem.* **2003**, *545*, 117–122.

(64) Vire, J. C.; De Jager, R. L.; Dupont, D. G.; Patriarche, G. J.; Christian, G. D. *Fresenius J. Anal. Chem* **1981**, *307*, 277–282.

(65) Kovala-Demertzi, D.; Domopoulou, A.; Demertzis, M. A.; Valdes-Martinez, J.; Hernandez-Ortega, S.; Espinosa-Perez, G.; West, D. X.; Salberg, M. M.; Bain, G. A.; Bloom, P. D. *Polyhedron* **1996**, *15*, 2587–2596.

this is the first detailed electrochemical study of the influence of metal ions and the chalcogen donor identity on the redox properties of thiosemicarbazones.

There are two locations, where the ligand-centered reduction of the complexes can take place: either at the C=N double bond of the 2-acetylpyridine moiety (CH_3C=N) or at the C=N double bond in close proximity to the chalcogen atom. By comparison of the ^{13}C NMR data of the gallium complexes **1A**−**1I** with the $E_{1/2}$ redox potentials, a good correlation can be found for both carbon resonances of the CH_3C=N moiety (Figures 9 and S2, Supporting Information); an increasing redox potential at $^{I}L^{red}$ and $^{II}L^{red}$ correlates with enhanced electronic deshielding resulting in downfield chemical shifts for the corresponding ^{13}C nucleus. This allows for the prediction of the ligand-centered redox potentials of the gallium complexes by NMR shifts, and vice versa. In contrast, no correlation could be found for the C−S resonance (**1A** 172.9 ppm; **1B** 176.1 ppm; **1C** 172.5 ppm; **1D** 172.4 ppm).[23,24] Therefore, we suppose that the one-electron ligand-centered reduction takes place at the CH_3C=N bond. This is in agreement with quantum chemical calculations (see below) and the chemical reduction of this C=N bond for the metal-free and coordinated ligands. The addition of $NaBH_4$ to an ethanolic solution of ligand $\mathbf{HL^B}$ resulted in the reduction of the C=N bond and the formation of ligand $\mathbf{HL^M}$, which displays its first reduction wave only at −2.10 V vs NHE. Similarly, reduction of the nitrate salt of **1B** (precipitated after addition of diethyl ether to the 1:2 mixture of $Ga(NO_3)_3$ and $\mathbf{HL^B}$) with $NaBH_4$ yielded a product containing the uncoordinated reduced ligand $\mathbf{HL^M}$ in around 50% yield.

Quantum Chemical Studies. Density functional calculations were performed to elucidate (i) why the ligand-centered reductions of the iron(II) complexes $[Fe^{II}(L)_2]$ (formed by reduction of the iron(III) complex $[Fe^{III}(L)_2]^+$) have a lower standard reduction potential (SRP) than the nonmetalated thiosemicarbazones (HL) and (ii) to locate the site of reduction at the thiosemicarbazone ligands. The reduction of a compound should be strongly facilitated by forming a complex with a cationic metal ion, which should have been reflected by a considerably higher redox potential. The one-electron-reduction events involving the species, $(\mathbf{L^B})^-$, $\mathbf{HL^B}$, $[Ga(\mathbf{L^B})_2]^+$ (**1B**), and $[Fe^{II}(\mathbf{L^B})_2]$ (**2B**), yielding their reduced forms, $(\mathbf{L^B})^{2-}$, $(\mathbf{HL^B})^-$, $[Ga(\mathbf{L^B})_2]$, and $[Fe^{II}(\mathbf{L^B})_2]^-$, respectively, have been investigated and compared. Note that the deprotonated species $(\mathbf{L^B})^-$ shall serve as the intuitive reference compound in our calculations, because the reduction potential of $(\mathbf{L^B})^-$ may be controlled by either protonation ($\mathbf{HL^B}$) or metalation ($[Ga(\mathbf{L^B})_2]^+$ and $[Fe^{II}(\mathbf{L^B})_2]$). Table 3 shows an excellent agreement of our calculated and experimental SRPs, validating the computational approach employed for this study (all energies and SRP values are calculated in acetonitrile solution).

Figure 10 displays the predicted structures of the most stable isomers of $(\mathbf{L^B})^-$, $\mathbf{HL^B}$, and their reduced forms, while other plausible isomers of $(\mathbf{L^B})^-$ and $\mathbf{HL^B}$ are shown in Supporting Information, Figure S3. Figure 10 also displays

Table 3. Calculated and Experimental Standard Redox Potentials (SRP, in V vs NHE), Hirshfeld Partial Charges in the Oxidized and Reduced Forms, and LUMO Energy Level of the Oxidized Species (E_{LUMO}, in eV)

			partial charges				
	SRP ($E_{1/2}$); $^{I}L^{red}$		ox		red		
compound	calcd	exptl	M^a	L	M^a	L	E_{LUMO}
$(\mathbf{L^B})^{-/2-}$	−1.69			−1.00		−2.00	1.12
$[Fe(\mathbf{L^B})_2]^{0/-}$	−1.56	−1.61	0.02	−0.01	0.02	−0.51	−2.45
$(\mathbf{HL^B})^{0/-}$	−1.12	−1.21	0.08	−0.08	0.07	−1.07	−3.03
$[Ga(\mathbf{L^B})_2]^{+/0}$	−0.86	−0.93	0.32	0.34	0.32	−0.16	−5.85

[a] H, Ga, and Fe, respectively.

Table 4. Calculated Metal−Ligand Bond Lengths in Ångstrom

	metal−S		metal−N(N−N)		metal−N(py)	
compound	ox	red	ox	red	ox	red
$[Ga(\mathbf{L^B})_2]^{+/0}$	2.41	2.45	2.09	2.06	2.14	2.12
$[Fe(\mathbf{L^B})_2]^{0/-}$	2.32	2.34	1.90	1.90	1.94	1.94

the structure of the gallium complex $[Ga(\mathbf{L^B})_2]^+$, while the other metal complexes have the same overall shape but with noticeable differences in the bond distances (see Tables 4 and S4, Supporting Information). The predicted structures of $\mathbf{HL^B}$ and $[Ga(\mathbf{L^B})_2]^+$ are in good to excellent agreement with available X-ray crystallographic structures (Supporting Information, Table S4). The calculations reveal structural changes in the entire compounds upon reduction. In the free ligand $(\mathbf{L^B})^-$ (Figure 10, top), the C−S bond is elongated (+0.04 Å) upon reduction, the adjacent C=N bond is shortened (−0.03 Å), the N−N bond is elongated (+0.03 Å), the acetylpyridine C=N bond is elongated (+0.03 Å), the adjacent C−C bond is shortened (−0.02 Å), and the C=N bond in the pyridine is elongated (+0.04 Å). Similar structural changes occur when the protonated species $\mathbf{HL^B}$ is reduced (Figure 10). Upon reduction of the metal complexes $[Ga(\mathbf{L^B})_2]^+$ and $[Fe^{II}(\mathbf{L^B})_2]$, the structures within the ligands change in a similar manner, but to a lesser extent as compared to the nonmetalated species (Supporting Information, Table S4). The reduction of the metal complexes is also accompanied by relatively minor changes in the metal−ligand distances (Table 4). The Ga−N bonds are slightly shortened (−0.02 and −0.03 Å), whereas the Ga−S bonds are elongated (+0.04 Å). In contrast, the Fe−N distances remain constant, while the Fe−S bonds are slightly elongated (+0.02 Å).

Table 3 lists the electron-density-based Hirshfeld partial charges on the ligands, the metals, and the proton in the four initial species and their reduced forms. The calculated charges at the H, Fe, and Ga atoms in $\mathbf{HL^B}$, $[Fe^{II}(\mathbf{L^B})_2]$, and $[Ga(\mathbf{L^B})_2]^+$ are +0.08, +0.02, and +0.32, respectively, while the charge on each ligand is −0.08, −0.01, and +0.34, adding up to a total charge of 0, 0, and +1 in these compounds. Upon reduction, the charges at H, Fe, and Ga remain constant, while the additional electronic charge is distributed over the ligands. Partial charges calculated using various other approaches are given in Supporting Information, Table S5. While the absolute values differ from the Hirshfeld charges, the overall trend of the charges increasing in the order Fe < H < Ga is supported by each approach. The intuitive assumption that the reduction of a compound

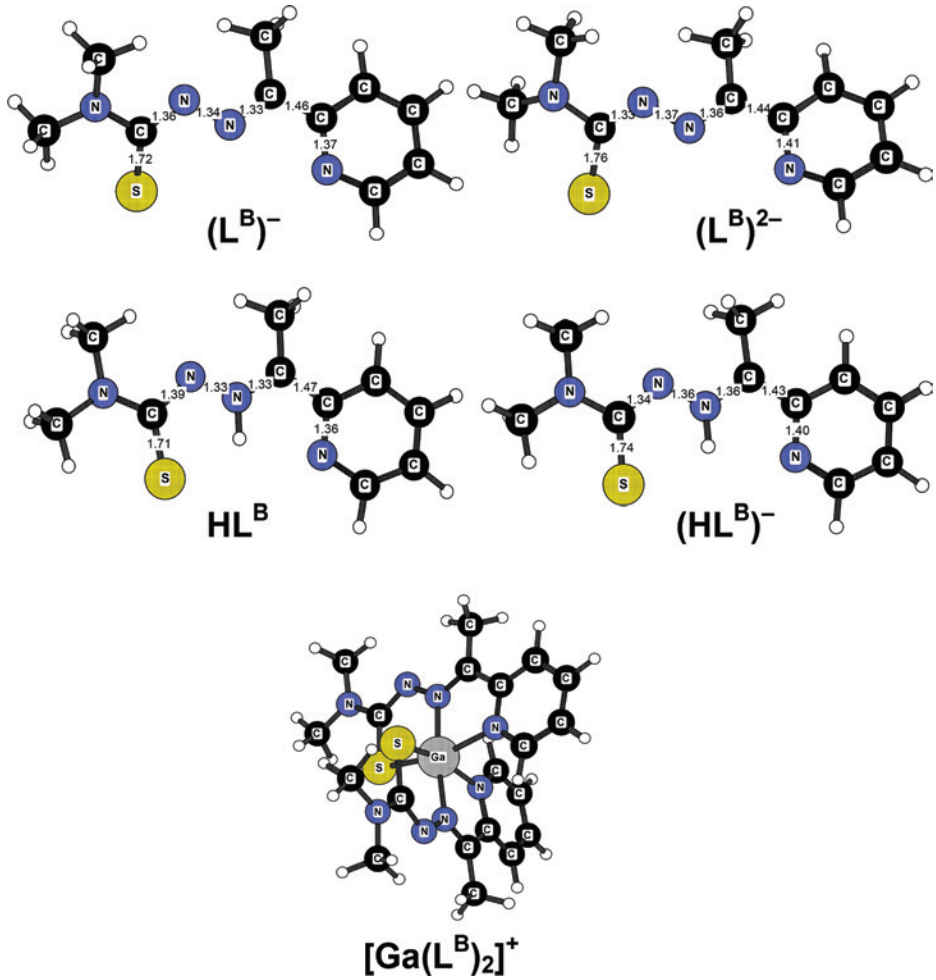

Figure 10. Calculated structures of $(\mathbf{L^B})^-$, $(\mathbf{L^B})^{2-}$, $\mathbf{HL^B}$, $(\mathbf{HL^B})^-$, and $[Ga(\mathbf{L^B})_2]^+$. Bond lengths in Å.

is facilitated when it binds to a metal ion appears to be valid only if the deprotonated free ligand $(\mathbf{L^B})^-$ is considered as the reference compound, whereas a proton promotes the reduction of the thiosemicarbazone more strongly than does the iron(II) ion with its d^6 low-spin electron configuration.

Figure 11 displays the semioccupied molecular orbital (SOMO) of the four reduced species $(\mathbf{L^B})^{2-}$, $(\mathbf{HL^B})^-$, $[Fe^{II}(\mathbf{L^B})_2]^-$, and $[Ga(\mathbf{L^B})_2]$. This orbital corresponds in each case to the lowest unoccupied orbital (LUMO) of the oxidized form (Supporting Information, Figure S4). The LUMO energy levels of the oxidized species are also listed in Table 3 and correlate with the reduction potentials: the lower the LUMO energy, the easier the reduction. The SOMO of $(\mathbf{L^B})^{2-}$ and its conjugate acid $(\mathbf{HL^B})^-$ are very similar; they are distributed over the entire π system and have both bonding and antibonding character leading to the bond distance changes upon reduction (see above). For instance, as the SOMO of $(\mathbf{HL^B})^-$ has a bonding contribution to the C═N bond adjacent to the sulfur atom (marked with b in Figure 11), this bond is shortened when an electron occupies this orbital. The SOMO of $(\mathbf{HL^B})^-$ has an antibonding contribution to the C═N bond adjacent to the pyridyl group (marked with a in Figure 11), thus elongating this bond upon reduction. This result is consistent with the chemoselective hydrogenation of the latter C═N bond by $NaBH_4$ (see above). The SOMO of the reduced metal complexes show the same bonding and antibonding patterns as those in the SOMO of the free ligand. In contrast to the SOMO of the gallium species, the SOMO of the reduced iron complex contains a small fraction of a metal d orbital. Note that none of the iron−ligand bond lengths shortens during reduction, indicating an enhanced Pauli repulsion between the ligand orbitals and the partially filled d shell in the reduced iron complex.

Biological Relevance and Comparison of Electrochemical Data with Cytotoxicity and R2 Specific Tyrosine Free Radical Quenching. The influence of water on the redox potentials of the gallium, iron, and ruthenium complexes was studied by measuring complexes **1B**, **1C**, **1G**, **1H**, **1I**, **2B**, **2C**, **2D, 2G**, **2H**, **2I**, and **3B** in CH_3CN/H_2O (7:3 v/v) or DMF/H_2O (7:3 v/v) mixtures. The low solubility of the complexes prevented the measurement in pure aqueous electrolyte solutions. The metal-centered redox waves for the $M^{III} \rightarrow M^{II}$ process for the iron and ruthenium complexes remained reversible (involving net 1+/0 net charged complexes) in the aqueous organic electrolyte solutions and are slightly shifted to more negative values with a maximum

(66) Richardson, D. R.; Sharpe, P. C.; Lovejoy, D. B.; Senaratne, D.; Kalinowski, D. S.; Islam, M.; Bernhardt, P. V. *J. Med. Chem.* **2006**, *49*, 6510–6521.

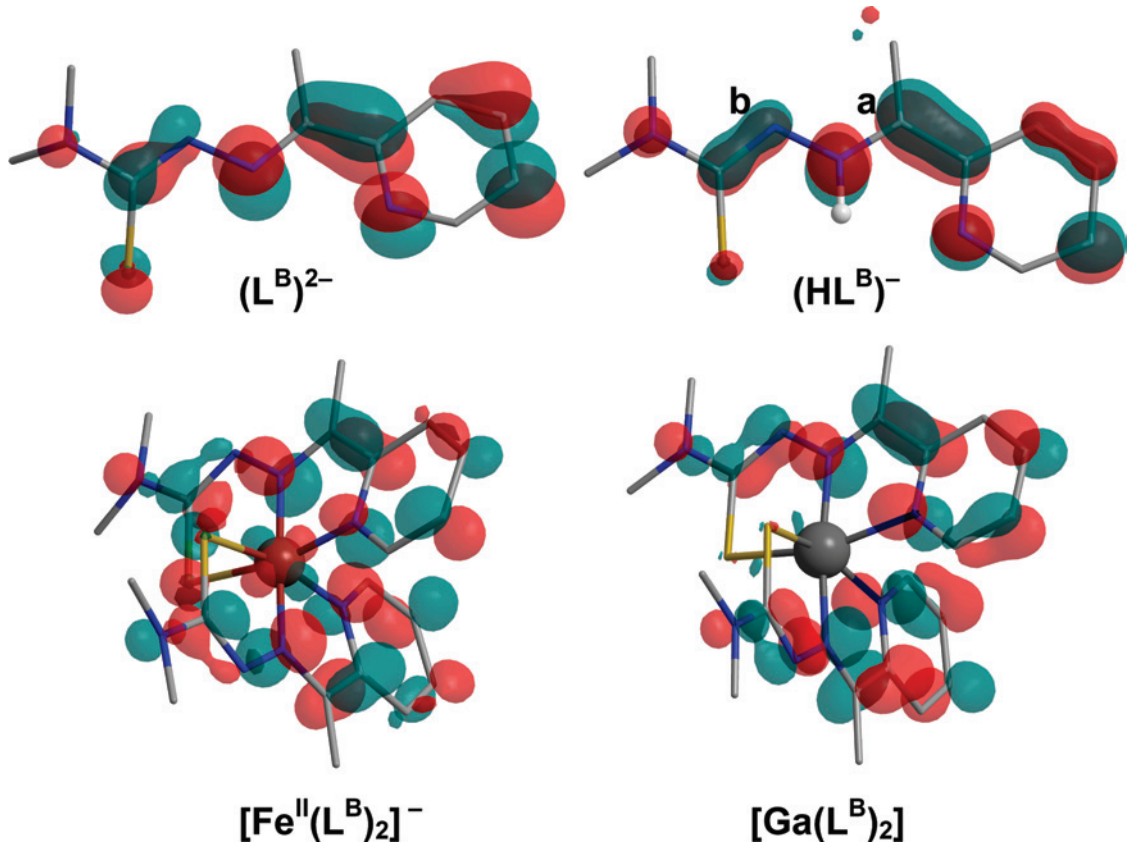

Figure 11. SOMO of the reduced species.

shift of −70 mV for **2D**. Iron dipyridinyl thiosemicarbazone complexes measured in CH_3CN/H_2O (7:3 v/v) were reported to give reversible Fe^{III}/Fe^{II} redox potentials of +0.153 to +0.225 V vs NHE.[66] The direct dipyridinyl analogs of complex **2B** and **2C** exhibit redox potentials of +0.166 and +0.225 V vs NHE, respectively, implying a more positive potential of the phenyl substituted complex in comparison to the ^4N-dimethyl-substituted one in line with our results. In general, higher potentials are observed for dipyridinyl complexes due to the electron withdrawing properties of the pyridinyl group. Furthermore, a series of 5-substituted 2-formylpyridine thiosemicarbazone complexes measured in water possess reversible iron redox potentials from +0.024 to +0.386 V vs NHE.[67]

Because water has a smaller potential window, the ligand-centered reductions for the iron complexes could be studied only in the case of **2G** and **2H**. These turned out to be completely irreversible indicating that the generated radicals upon reduction can no longer be stabilized by the metal center resulting in fast radical quenching by the water. We can therefore assume that the generated ligand-radicals are highly reactive under physiological conditions. In contrast to the iron-centered redox processes, the reduction potentials (E_p) for the first ligand reduction (wave $^{I}L^{red}$; involving net 0/1− charged complexes) is shifted by +100 mV and for the second ligand-centered reduction (wave $^{II}L^{red}$; involving net 1−/2− charged complexes) by approximately +300 mV for both complexes compared to the measurements in CH_3CN electrolyte solutions. The first ligand-centered reduction potential (wave $^{I}L^{red}$; involving net 1+/0 net charged complexes) of the gallium complexes **1B**, **1C**, **1G**, **1H**, and **1I** showed a slightly cathodically shifted redox potential (ca., −50 mV), whereas the second ligand-reduction at $^{II}L^{red}$ was anodically shifted up to +150 mV compared to the measurements in pure organic electrolyte solutions. In general, redox couples involving positive net charged species are shifted to more negative redox potentials in aqueous solutions (compared to organic medium) and vice versa. This behavior has been explained previously[1,10] on the basis of the Born model of solvation. In accordance with this model, stabilization of a more positively or more negatively charged species occurs through the higher solvation energy of water resulting in decreasing or increasing redox potentials, respectively. The Born equation shows that the solvation energy is proportional to the squared charge, what explains the larger shift for the 1−/2− charged species (wave $^{II}L^{red}$ in iron(II) complexes) compared to the 0/1− and 1+/0 net charged complexes.

The physiological accessibility of the M^{III}/M^{II} redox couple between 0.06 and 0.51 V vs NHE by biological reducing agents was studied by UV−vis spectroscopy measurements of complexes **2B**, **2G**, and **3B** in 1% aqueous DMSO solution with a 5-fold excess of ascorbic acid ($E_{1/2}$ = +0.06 vs NHE[68]). Complex **2G** is reduced immediately after addition of ascorbic acid accompanied by a color change from brown to green. For the ruthenium(III) complex, the UV−vis spectrum changes within minutes, whereas for **2B** only small

(67) Knight, J. M.; Whelan, H.; Petering, D. H. *J. Inorg. Biochem.* **1979**, *11*, 327–338.
(68) *CRC Handbook of Biochemistry and Molecular Biology*; Fasman, G. D., ED.; CRC Press: Cleveland, OH, 1976; p 122.

changes can be observed after hours. These results are in accordance with the M^{III}/M^{II} redox potentials of the metal complexes. One major goal of this study was to introduce electron-withdrawing substituents such as nitro-groups into the thiosemicarbazone ligands to shift the ligand-centered redox potentials in the direction of the physiologically accessible range. Indeed, several gallium complexes have redox potentials for $^{I}L^{red}$ around −0.4 vs NHE, which is given as a guiding value for the redox potential reachable in cells.[69] Unfortunately, the low solubility in DMSO/H_2O mixtures with a maximal content of 1% DMSO prevents the cytotoxicity measurements of the novel synthesized compounds. Therefore the comparison of the IC_{50} values and the electrochemical data can only be done for the ^4N-disubstituted ligands and complexes. The cytotoxicity data of the 41 M cancer cell line show the overall trend that the iron(III) complexes exhibit the lowest cytotoxicity (13−172 nM) followed by the metal-free ligand (0.073−1.1 nM) and the gallium complexes (0.0045−0.27 nM).[23] The same trend, but less pronounced, can be found in the SK-BR-3 cancer cell line.[23] The direct comparison reveals that the gallium(III) complexes are by a factor of 210 to 33000 (41M) and 150 to 4000 (SK-BR-3) more cytotoxic than the corresponding iron complexes, respectively. Interestingly, the coordinated thiosemicarbazone ligands are most easily reduced in the case of the gallium complexes, followed by the metal-free ligands and shifted to very low redox values in the case of the iron complexes, what correlates with the previously obtained cytotoxic data. But as mentioned above, we should be aware that the physiologically accessible range of the redox potential of cells is given from −0.4 to +0.8 V vs NHE.[69] The order of the R2 specific tyrosine free radical destruction in mouse ribonucleotide reductase is in contrast to the cytotoxicity data and the electrochemical results of the ligand-centered reductions: fastest inhibition of the enzyme occurs in the case of the iron complexes suggesting that the redox properties of iron play an important role in the radical quenching process.

Final Remarks

The syntheses of a series of gallium-, iron-, and ruthenium-chalcogensemicarbazonate complexes are reported; the electrochemical properties of these compounds are investigated in detail, and their biological relevance is discussed. The electrochemical behavior of these complexes can be specified by (i) physiologically accessible metal-centered redox potentials for the iron(III) and ruthenium(III) complexes, (ii) formation of stable ligand radicals on the time-scale of cyclic voltammetry upon reduction of the noninnocent chalcogensemicarbazone ligands in aprotic solvents, (iii) quenching of these reductively induced ligand radicals by water, (iv) shift of the ligand-centered redox potential in the physiologically accessible range for some gallium complexes when electron-withdrawing moieties are incorporated into the ligand, and (v) ligand-reduction for the gallium complexes occurs at the $CH_3C{=}N$ double bond. Quantum chemical calculations show that reduction of the coordinated and metal-free thiosemicarbazone ligands occurs at a π-orbital that spreads over the entire thiosemicarbazone moiety. The ligand-centered reductions $^{I}L^{red}$ and $^{II}L^{red}$ take place at 0.3−0.8 V more positive potentials for the gallium complexes than for the uncoordinated (protonated) ligands. The latter on the other hand are easier to reduce than the corresponding iron(II) complexes. The redox potentials increasing in the order $[Fe^{II}(L^B)_2] < HL^B < [Ga(L^B)_2]^+$ are consistent with the trend of the calculated partial charges, Fe < H < Ga, in these compounds and with the energy levels of their LUMO. The presented results on the electrochemical behavior of potential antitumor chalcogensemicarbazonate complexes allow for the future design of potential drugs with predictable and desired redox properties.

Acknowledgment. The authors are indebted to the FWF (Austrian Science Fund), to the Austrian Council for Research and Technology Development and COST (European Cooperation in the Field of Scientific and Technical Research) for financial support. We also thank Anatoly Dobrov for the measurement of mass spectra, and Alexander Roller for the collection of the X-ray data.

Supporting Information Available: Detailed discussion of the NMR data of **1H**, redox potentials of the metal-free ligands $\mathbf{HL^A}-\mathbf{HL^M}$, cyclic voltammogram of **3B** with ligand centered reductions and plot of $\delta(^{13}CH_3)$ of the $CH_3C{=}N$ moiety versus $E_{1/2}$ of complexes **1A**−**1H**, calculated relative energies of plausible isomers of $\mathbf{HL^B}$ and its deprotonated form, calculated bond lengths and partial charges of $(\mathbf{L^B})^-$, $\mathbf{HL^B}$, $[Fe^{II}(\mathbf{L^B})_2]$, $[Ga(\mathbf{L^B})_2]^+$, and their one-electron reduction products, plots of the LUMO of the reduced species, comparison of the standard reduction potentials calculated at B3LYP and BP86, relative energies of plausible electronic states of $[Fe^{II}(\mathbf{L^B})_2]$ and $[Fe^{II}(\mathbf{L^B})_2]^-$, and X-ray crystallographic files in CIF format for $\mathbf{HL^H}$, $\mathbf{HL^M}$, and $\mathbf{1H}\cdot H_2O$. This material is available free of charge via the Internet at http://pubs.acs.org.

IC8013249

(69) Kirlin, W. G.; Cai, J.; Thompson, S. A.; Diaz, D.; Kavanagh, T. J.; Jones, D. P. *Free Radical Biol. Med.* **1999**, *27*, 1208–1218.